AD

TECHNICAL REPORT ARCCB-TR-96009

EFFECTS OF THERMAL TREATMENT AND LOADING RATE VARIATION ON GRAPHITE BISMALEIMIDE

ALICE E. FISH

APRIL 1996

US ARMY ARMAMENT RESEARCH,
DEVELOPMENT AND ENGINEERING CENTER
CLOSE COMBAT ARMAMENTS CENTER
BENÉT LABORATORIES
WATERVLIET, N.Y. 12189-4050

DISCLAIMER NOTICE

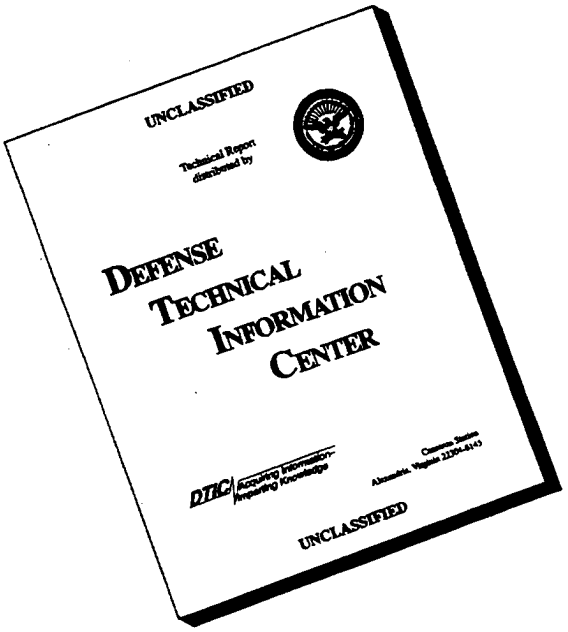

THIS DOCUMENT IS BEST QUALITY AVAILABLE. THE COPY FURNISHED TO DTIC CONTAINED A SIGNIFICANT NUMBER OF PAGES WHICH DO NOT REPRODUCE LEGIBLY.

DISCLAIMER

The findings in this report are not to be construed as an official Department of the Army position unless so designated by other authorized documents.

The use of trade name(s) and/or manufacturer(s) does not constitute an official indorsement or approval.

DESTRUCTION NOTICE

For classified documents, follow the procedures in DoD 5200.22-M, Industrial Security Manual, Section II-19 or DoD 5200.1-R, Information Security Program Regulation, Chapter IX.

For unclassified, limited documents, destroy by any method that will prevent disclosure of contents or reconstruction of the document.

For unclassified, unlimited documents, destroy when the report is no longer needed. Do not return it to the originator.

REPORT DOCUMENTATION PAGE

Form Approved
OMB No. 0704-0188

1. AGENCY USE ONLY (Leave blank)	2. REPORT DATE	3. REPORT TYPE AND DATES COVERED
	April 1996	Final

4. TITLE AND SUBTITLE
EFFECTS OF THERMAL TREATMENT AND LOADING RATE VARIATION ON GRAPHITE BISMALEIMIDE

5. FUNDING NUMBERS
AMCMS No. 6126.24.H180.0

6. AUTHOR(S)
Alice E. Fish

7. PERFORMING ORGANIZATION NAME(S) AND ADDRESS(ES)
U.S. Army ARDEC
Benet Laboratories, AMSTA-AR-CCB-O
Watervliet, NY 12189-4050

8. PERFORMING ORGANIZATION REPORT NUMBER
ARCCB-TR-96009

9. SPONSORING / MONITORING AGENCY NAME(S) AND ADDRESS(ES)
U.S. Army ARDEC
Close Combat Armaments Center
Picatinny Arsenal, NJ 07806-5000

10. SPONSORING / MONITORING AGENCY REPORT NUMBER

11. SUPPLEMENTARY NOTES

12a. DISTRIBUTION / AVAILABILITY STATEMENT
Approved for public release; distribution unlimited.

12b. DISTRIBUTION CODE

13. ABSTRACT *(Maximum 200 words)*

In this work, the tensile properties of graphite-reinforced bismaleimide were studied. In particular, specimen design, loading rate variation, and thermal exposure effects were examined on a series of specimens. The purpose of this study was twofold: (1) develop a tensile specimen design that provides consistent, reliable data; and (2) provide a foundation for evaluating the mechanical behavior aspects of this composite system. Several issues associated with tensile design in regard to tensile specimens were considered, including specimen thickness, fiber orientation, specimen shape, tab material selection, and extensometer/strain gage incorporation. The analysis indicated that tab angle played a significant role in the resulting stress-to-failure data. By using a straight-sided specimen, appropriate specimen thickness, carefully fixturing the composite specimen in the wedge grips and using 15° tab angles, reliable test data were generated.

Mechanical property data, in the form of stress-to-failure values, were generated by the tensile tests. Two thermal treatments, representing certain service conditions, were selected and compared to a base line (as-cured) condition. These thermal treatments were shown to have had an effect on the stress-to-failure results. The data indicated that thermal exposure caused a small reduction in the stress-to-failure values. Subjecting the composite to elevated temperatures resulted in an increased number of microcracks formed within the brittle matrix. Loading rate variation (0.22 mm/sec and 121 mm/sec) did not have a significant effect on the resulting mechanical property data. In order to identify the effects of the variables that were incorporated into the testing, a computer program designed to perform a linear regression analysis was utilized. It was apparent from the program that failure mode, thermal treatment, and individual composite plates, where tensile samples were obtained, played important roles in the final stress-to-failure results. The highest stress-to-failure values were obtained from the as-cured condition, uniform thickness of the tensile specimen (i.e., located near center of composite plates), and failures that resulted in "brooming."

14. SUBJECT TERMS	15. NUMBER OF PAGES
Graphite Bismalemide, Prepreg, Brooming, Debonding, Splitting	72
	16. PRICE CODE

17. SECURITY CLASSIFICATION OF REPORT	18. SECURITY CLASSIFICATION OF THIS PAGE	19. SECURITY CLASSIFICATION OF ABSTRACT	20. LIMITATION OF ABSTRACT
UNCLASSIFIED	UNCLASSIFIED	UNCLASSIFIED	UL

TABLE OF CONTENTS

TABLES

LIST OF ILLUSTRATIONS

ACKNOWLEDGEMENTS

I would like to express my great appreciation to Dr. Roger N. Wright for providing me with the educational opportunity in helping to fulfill my goal of obtaining my Masters degree. I would also like to extend a special thanks to Eric Leighton and Dan Crayon, whose help made this research both enjoyable and educational. I additionally would like to thank Victor Montuori, who assisted me with the statistical analysis of the test data. Lastly, I wish to thank my family for providing me with love, encouragement, and support throughout this endeavor.

1.0 INTRODUCTION

Engineering of composite materials has added a new dimension to the advancement of materials science. The need for low density, high strength materials is apparent in major industries including aerospace, transportation, biomedical, and defense.

Composite systems, including polymer matrix composites (PMC), metal matrix composites (MMC), and ceramic matrix composites (CMC) reinforced with fibers, whiskers, or particles, have been established as viable alternatives to metal components for certain applications. As with any material consideration, the selection of a candidate material depends upon the intended application. The ability to create a unique material by changing variables within a given composite system, enables the user to tailor the end product in order to optimize desired properties.

Continuous-carbon-fiber polymer matrix composites are rapidly finding their way into high performance applications, which require elevated temperatures, low densities, and high strength levels. A primary example of one such research directive requiring stringent performance levels is apparent in the development of composite overwraps or jackets for gun tubes. In the case of a pressure vessel, environmental integrity, as well as high temperature capabilities, is an essential consideration in the design of an effective component. The constraints surrounding this particular effort exist in the form of environmental considerations, differential thermal expansion coefficients between metal and composite, thermal integrity, and loading rate effects affecting the composite.

The primary objective for the current work is based upon the need to generate information about graphite bismaleimide in order to effectively facilitate the use of this composite system in various applications. This study was initiated in order to study the effects of tensile design, high loading rates, and thermal exposure on graphite bismaleimide. Through this effort, we are hoping to gain further insight regarding the behavioral aspects of this composite system.

2.0 HISTORICAL REVIEW

2.1 Polymeric Materials

Polymers play an integral role in the manufacturing of products in the world today. The extensive use of polymers can be attributed to their cost effective processing, excellent environmental resistance, and low densities. However, many polymeric materials are limited by temperature, strength, and brittleness. In order to circumvent some of these limitations, polymer scientists developed polymeric materials exhibiting high glass transition temperatures which are commonly referred to as polyimides. The stability of this type of polymer is related to the formation of interconnected networks, i.e., crosslinking, and is typically referred to as a thermoset. In order to create these vast crosslinked networks, a chemical reaction must occur, hence, heat must be supplied to initiate the process. The polymers that are created through the process of polymerization are focused into two primary groups: condensation or addition polymers. The bismaleimides are classified under the addition-type polyimides and were first successfully produced in the year 1968. The bismaleimide resin was developed with the intent of producing a polymer with high service temperature ranges reaching ~200°C. However, a significant drawback of this particular matrix system is centered around its inherent brittleness.

2.2 Graphite Fibers

The term "graphite" was created in order to differentiate between graphite fibers, which contain carbon contents in excess of 99%, versus carbon fibers, which are

typically in the range of 80% to 95% carbon. In addition, graphite fibers typically exhibit higher moduli and higher tenacity, which leads to greater thermal and electrical conductivity in the material.

Graphite fibers serve as the predominant form of reinforcement for polymer matrix composites. The high strength and high modulus of the fibers provide the composite with excellent performance capabilities. The graphite structure is composed of carbon atoms arranged in densely packed hexagonal layers. The bonds connecting the atoms in the layer plane are extremely strong, leading to a high strength modulus. However, the bonds that connect the neighboring layers are comprised of weak van der Waal-type forces, thereby resulting in a somewhat lower modulus in that particular direction.[1]

As the demand for "high performance" materials continues to increase, utilization of fiber-reinforced composites becomes more of a necessity as an alternative material. Graphite fibers are very popular due to their excellent properties, which include good corrosion resistance, low density, resistance to degradation at high temperatures, and high tensile strengths. However, graphite fibers do not serve as a panacea for detrimental effects such as high temperature oxidation, which can be encountered in thermally-dependent service environments.

2.3 Characteristics of Fibrous Composite Systems

The most unique feature of a composite system is the ability to combine two or more materials in order to create a desired set of properties. Typically, fibrous composites are comprised of matrix and reinforcement.

The primary role of the matrix is to transfer the load to the fibers. The matrix also serves as a binder to hold the fibers together, in addition to protecting the reinforcement from environmental degradation. Although the matrix plays a vital role in the overall composite performance, the reinforcement provides the strength.

Fiber reinforcements are the "backbone" of the material. The function of continuous reinforcement is threefold: small fiber diameters which permit higher theoretical strengths to be achieved and decrease the probability of imperfections in the material; high aspect ratios which permit load transfer from matrix to stiff/strong fibers; and high degree of flexibility which arises from the fact that the fiber exhibits a high modulus and small diameter. The flexibility of a material is a function of the elastic modulus and the moment of inertia of its cross section.[1] The strength of the fabricated composite is highly dependent on the stacking sequence of the laminae. The stacking sequence for a composite system can be defined by the following code: $[0_2/90_4/0_2]$. This code implies that starting from the bottom of the laminate, at z = -h/2, we have a group of two plies at the 0° orientation, followed by four plies in the 90° direction, and lastly two additional plies in the 0° direction in order to balance the laminate to prevent warpage from occurring during the curing process. Another example would be a simple case of $[90_8]$, which implies that eight layers are layed-up in the 90° direction.

2.3.1 Fracture Modes in Continuous Fiber-Reinforced Composites

There are three basic fracture modes in which one may describe failure of fiber-reinforced composites: interlaminar, intralaminar, and translaminar.

Interlaminar failure describes a type of fracture that occurs parallel to the fiber reinforcement and results in brittle matrix failure. The "river marks," which are formed as a result of the brittle matrix failure, correspond to microscopically displaced failure planes in the form of fracture ridges. Crack progression within these areas causes the ridges to link together, resulting in the formation of a river-like pattern.

Intralaminar failure is similar to interlaminar failure in that fracture occurs parallel to the fiber reinforcement. This type of failure mode is defined as failure occurring internally within a ply.

Translaminar failure can be described as a type of failure that is characterized by rough, fiber-dominated morphologies. The operative separation mechanisms for translaminar failure are considered to originate from either tensile stresses or compressive microbuckling. Macroscopic observations[2] of translaminar tension fractures tend to exhibit numerous fibers projecting from the main fracture plane with little evidence of delamination. Fibers tend to fracture in groups or bundles, with failure occurring in one of three forms: fiber pull-out, fiber end fracture, or matrix fracture. In contrast to interlaminar failure, which typically forms a distinct crack front, fracture via translaminar failure occurs as a result of the formation of multiple initiation zones, whereby all fiber breaks originate from a single source.

2.3.2 Damage Development in Orthotropic Polymer Composites

Damage development prior to failure is evident in the form of matrix cracking. The growth of these cracks is believed to originate from inherent flaws within the material, such as fiber/matrix debonds or matrix voids. Under applied loading or temperature changes,

the flaws behave as local stress risers. Harrison and Bader[3] conducted monotonic tensile tests on the effects of cracking on transverse ply thickness variations of [0°/90°/0°]. Upon increasing the transverse thickness of the composite, a subsequent decrease in failure stress due to extra cross-sectional area in the transverse direction occurred without an effective increase in the stiffness of the composite. The occurrence of transverse ply cracking originated from fiber/resin debonding. Upon increasing the stress, the fiber/resin debonds appeared to extend across the ply thickness, thereby forming a transverse crack. The experimentation revealed that the cracking which occurred in the transverse layers originated from the edges of the test coupon. The authors additionally noted that the degree of transverse cracking was dependent on the transverse thickness. The formation of cracks from the fiber/resin debonds appeared to be constrained by small transverse ply layers. It was also noted that initiation (fiber/matrix debond) and propagation (cracking) occurred almost simultaneously, whereas the smaller plies diminished the propensity for crack extension. Initiation of cracking in the 90° plies can be noted by a change in the stress-strain behavior indicating that the transverse strain is exceeded and microcracking in the transverse plies has begun. This phenomenon is referred to as first ply failure (FPF) and results in a reduction of the stiffness in the composite laminate.[4]

2.3.3 Strain Rate Effects of Graphite-Reinforced Polymer Composites

Studies on strain rate effects of graphite-reinforced polymer composites have been very limited. However, as applications for polymer composites are realized, the material response within a certain environment becomes vital. Daniel et al.[5] conducted experiments on

characterizing the effects of varying strain rates ranging from quasi-static to over $500s^{-1}$ on thin pressurized rings composed of graphite epoxy. The properties that were obtained via testing in the longitudinal direction $[0_6]$ revealed some interesting results. The modulus of the composite material showed a significant increase with increasing strain rate (up to 20%); whereas dynamic strength, ultimate tensile strain, and Poisson's ratio do not vary significantly with strain rate variations. Additional testing was performed on $[90_8]$ transverse rings. The testing again indicated an increase in modulus with increasing strain rates. More importantly, an increase in the transverse tensile strength was observed with an increase in strain rate, with values achieving two or three times the corresponding static values. In another paper written by Suvorova et al.[6], the effect of varying loading rates on orthogonally carbon-reinforced plastic was researched and discussed. The experiments indicated that an increase in strength was observed with increasing loading rates.

A comparison of these two papers indicates that the effects due to increases in loading rate (strain rate) are dependent upon the layup orientation.

2.4 Introduction to Graphite Bismaleimide (Gr/BMI)

Graphite bismaleimide is a polyimide matrix composite that exhibits excellent mechanical properties and retains thermal stability at high temperatures. However, these lucrative properties are offset by the fact that BMI composites exhibit poor impact damage resistance and out-of-plane tensile properties.

2.4.1 Generation of Thermal Strains in Gr/BMI Composite

The manifestation of microcracks within the composite material is directly related to the thermal stresses and strains produced by thermal exposure. The thermal strains that develop in BMI composite material are directly related to the thermal expansion coefficient of the fiber and the matrix. In addition, residual strains develop in cross-ply laminates (O°/90°) due to the expansion mismatch resulting from the differing orientations. These residual strains encourage the formation of microcracking within the laminates. A study performed by Simpson et al.[7] demonstrated that the differences between the linear expansion coefficients of the matrix and fiber may be of sufficient magnitude such that the transverse failure strain of the carbon-fiber composite is surpassed, resulting in the formation of microcracks. The authors additionally observed that the amount of thermal strain generation appeared to be dependent on the temperature of the post-cure. Post-cure temperatures of 340°C diminished the amount of strain generated within the laminates of O°/90° beams. Lower post-cure temperatures showed greater propensity for residual strains after thermal cycling. Post-cure temperatures exceeding 340°C resulted in microcracking.

The manifestation of thermal strains may also arise due to a temperature variation resulting in dimensional changes occurring between the fiber and the matrix. Unlike isotropic bodies, which contain one coefficient of thermal expansion (CTE), unidirectional composites have both longitudinal and transverse coefficients of thermal expansion.[1] The longitudinal CTE is typically small due to the mechanical constraint that the fibers impose on the matrix. At low fiber volume fractions, the transverse CTE may exceed the matrix coefficient resulting in an imposed tensile force on the matrix in the lateral direction.[8] These

differences in CTE may result in stresses forming within the laminate. The thermal strains that are generated as a result of CTE mismatch, in a graphite bismaleimide composite, cause microcracking to occur within the brittle matrix.

2.4.2 Thermo-Oxidative Stability of Gr/BMI Composite

According to Scola[9], thermal stability at elevated temperatures of graphite bismaleimide is dependent on two fundamental aspects of the composite system which include, "(1) the thermal and thermo-oxidative stability of the individual components and (2) the influence of the interface region between fibers and matrix on matrix stability." Previous studies, which have been performed on thermal stability at elevated temperatures over specified time durations, have shown that the fiber/matrix interface nearest to the external surface appears to degrade as a result of thermo-oxidative effects. Scola focuses on the effect that graphite fiber impurities, such as alkali metal ions, sodium, and potassium, have on the thermal oxidation progression. Scola contends that the graphite fiber surface impurities affect the bond integrity between the fiber and matrix. This has a significant effect on the thermo-oxidative stability. It has been observed that during aging, deterioration of the fiber/matrix interface occurs, thereby exposing the fibers to thermo-oxidative degradation.[4] Therefore, a fiber/matrix interface that exhibits good bond integrity will allow for greater thermo-oxidative stability.[10]

Bowles and Nowak[11] conducted studies on the influence of thermo-oxidative resistance on the fiber/matrix of PMR-15 reinforced with Celion 6000 (graphite fiber). The experiment was designed to investigate the influence of long-term exposure (700 to 1000

hours) at various temperatures, 288°, 316°, 329°, and 343°C. The authors noted the occurrence of surface crazing leading to microcracking on the composite surfaces that were exposed to the thermal treatments. Weight loss measurements consisted of observing the degradation and oxidation effects on each constituent individually and together as a composite. The weight loss per unit area, as shown in Figure 2.1 below, indicates that the resin was significantly more sensitive to thermal degradation than the graphite fiber was. However, the activation energy of the composite is higher than both that of the fiber and resin alone. The authors suggest that the fiber/matrix interaction together may have a synergistic effect on the thermal behavior of the composite material, thereby accounting for the increased activation energy. It was additionally observed that the fiber/matrix interface is very reactive in the presence of oxygen.

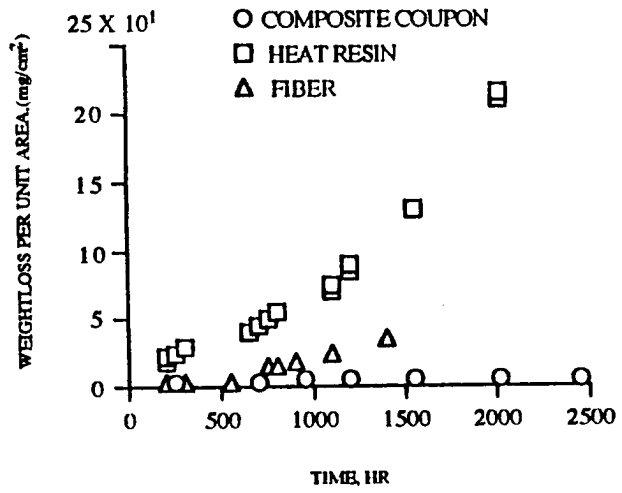

Figure 2.1 Weight loss per unit area (mg/cm^2) versus time (hr).

2.4.3 Thermal Exposure Effects on Gr/BMI

The effects of thermal exposure on graphite bismaleimide have been performed in order to study composite response. Many papers have been dedicated to the effect of microcracking in response to thermal treatment of polymer composites reinforced with graphite. A study conducted by Haskins and Kerr[12] illustrated the effects of thermal exposure at various time and temperature combinations on graphite-reinforced HT-S710 and Celion 6000/LARC-160 polyimide systems. Metallographic evidence indicated that the degree of microcracking within the matrix was related to the temperature and duration of exposure. It was noted that higher temperatures (273°C) for shorter time durations (10,000 hours) resulted in a greater degree of microcracking and oxidation effects, as compared to a sample exposed to a 218°C thermal exposure for 50,000 hours. The same study compared the effects of thermal exposure on tensile strength. It was shown that at a temperature of 218°C for 25,000 hours of exposure, little change in the tensile strength was observed. However, when the tensile specimen was exposed to a temperature of 273°C for 5,000 hours, a significant drop in tensile strength was observed. Metallographic studies of these specimens indicated that the degree of matrix degradation and oxidation was dependent on the exposure temperature. Scanning electron microscopic examinations revealed that the specimens aged at 218°C did not exhibit oxidation or matrix degradation effects for the first 25,000 hours. Upon increasing the temperature to 273°C, a significant amount of matrix degradation was observed.

Additional work on the effect of thermal exposure on graphite fabric/PMR-15 composites has been performed by Hanson and Serfini.[13] The experiment involved the addition of boron powder in the matrix of PMR-15 as a means of protecting and enhancing

composite properties. The experiments, which were conducted at 288°C, revealed a significant improvement in mechanical properties, i.e., flexural strength, flexural modulus, and interlaminar shear strength, due to the addition of boron powder. However, there did not appear to be any improvement in the oxidation resistance as a result of the boron impregnation.[13] Microscopic examination of long-term exposure (up to 1500 hours at 316°C) revealed that the samples that were exposed to the boron powder did not exhibit significant microcracking; whereas the samples without the boron powder, which underwent similar thermal treatment, exhibited extensive microcracking.

3.0 OBJECTIVES

Graphite bismaleimide is an attractive candidate for component design applications, due to its high temperature capabilities and thermal stability. A rigorous investigation of the tensile properties of Gr/BMI is required for sophisticated applications development. Thus, the principal objectives of this work are:

a. To develop a practical method of tensile testing reinforced polymeric composites.

b. To develop a statistical model in order to identify the primary influences that significantly affect the stress-to-failure results.

c. To incorporate a tab material/configuration that provides consistent, reliable data.

d. To evaluate the effects of thermal exposure on the Gr/BMI composite material.

e. To compare effects of dynamically tested specimens to their statically tested counterparts.

4.0 EXPERIMENTAL PROCEDURE

4.1 Material Processing of Gr/BMI

This section will address the composite condition received. In addition, the processing methods, cure cycle, and thermal treatments that the graphite bismaleimide was subjected to, will be discussed.

4.1.1 Prior History

The bismaleimide prepreg was produced by Amoco Performance Products. The resin system, utilized as the matrix material, was a bismaleimide MR-56-2. Carbon fiber (Type T650-42) strands were creeled and spread. They were then submerged into the bismaleimide resin bath, which was subsequently processed to a partially cured state (commercially referred to as "B" stage). The thickness and width of the prepreg tape were measured to be 0.012 cm and 15.24 cm, respectively.

4.1.2 Composite Layup

The BMI prepreg tape was cut into 30.5 cm strips, which were layed up in a predominantly uniaxial or "0" direction. The layup consisted of nine layers, where the fifth layer was rotated 90° or $[0_4,90_1,0_4]$. The laminate sheets were layed up in-between two 35.6 x 35.6 cm treated aluminum plates. After layup completion, the material was bagged and sealed. The composite plate fabrication process entailed the following steps:

- Sprayed aluminum plates with release agent, i.e., silicon - dry lubricant.

- Covered aluminum plates with solid-seal ply in order to prevent the resin from sticking to the mold. Solid-seal ply is a type of transparent material, similar to saran wrap.
- Layed up composite material onto aluminum plates.
- Taped edges of plates together to prevent movement from occurring.
- Encased aluminum plates in bleeder cloth. This cloth is a woven material used to enable excess gases and resin to escape during the composite curing process.
- Placed the composite plate inside a bagging material. The bagging material is an impermeable layer of film, which is placed over the uncured part. The bag is sealed such that a vacuum can be drawn.
- Placed a thermocouple within the bag in order to monitor the composite plate temperature.
- Vacuum sealed the bag.
- Placed composite into a preprogrammed autoclave.

4.1.3 Cure and Post-Cure Processing

The composite processing was performed in a Lipton autoclave with a nitrogen atmosphere. The autoclave was programmed to a cure cycle recommended by Amoco Performance Products, the supplier of the prepreg material. The cure cycle was performed according to the three graphs illustrated in Figure 4.1. The post-cure treatment, as recommended by the vendor, was performed in the autoclave for 14.5 hours in air. The oven/plate temperature was monitored by placing a thermocouple on one of the composite plates. After the designated time period, the pressure vessel was powered off and the plates

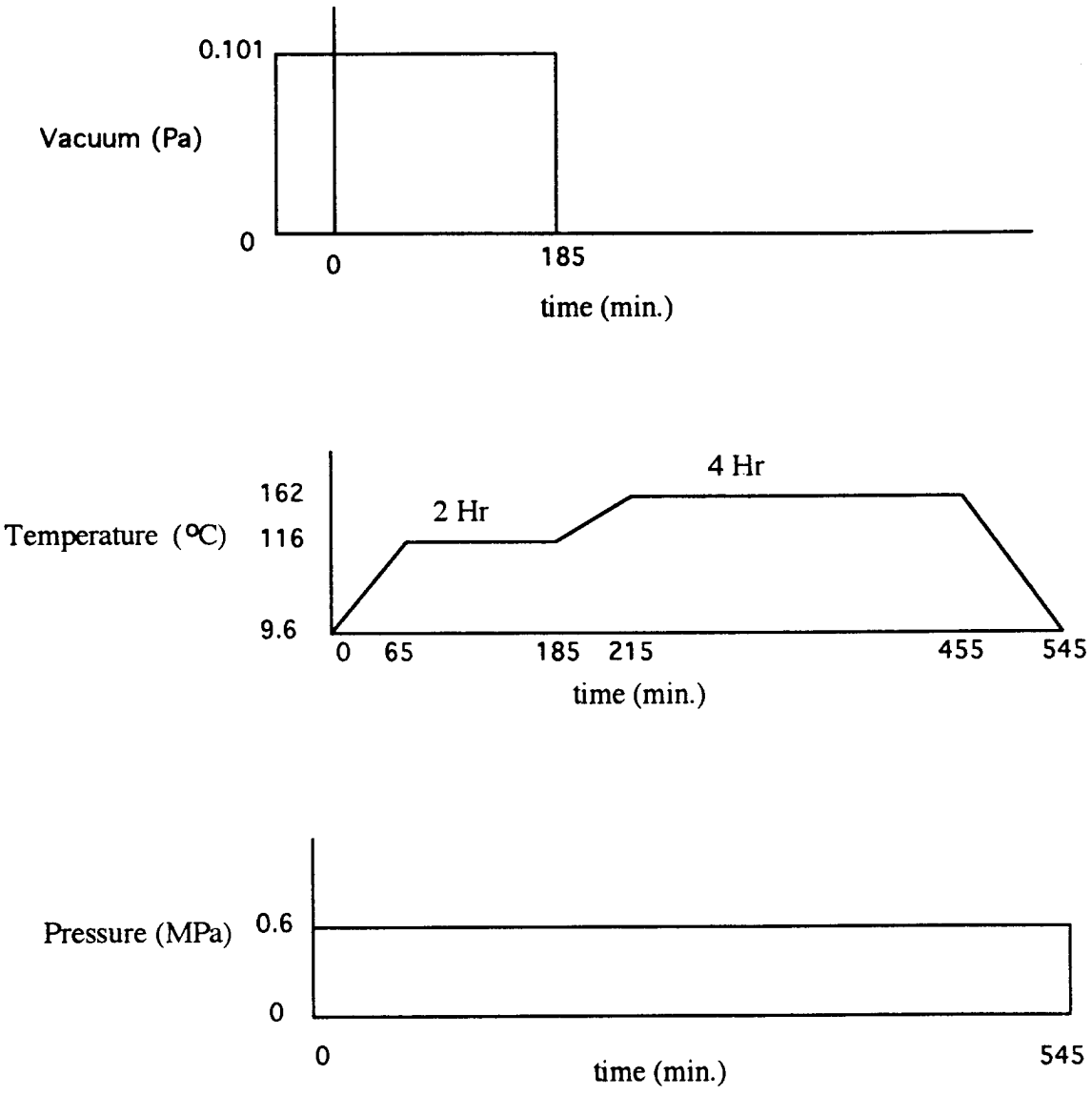

Figure 4.1 Autoclave Cure Cycle for T650-42/MR-56-2-Composite Material

were subjected to a furnace cool with a ramp down of 5°C/min. Figure 4.2 depicts a macrograph of the composite plate after the cure cycle was completed.

4.2 Thermal Treatment

The composite plates were subjected to a series of thermal treatments, which simulated the chrome plating process of U.S. Army gun tubes. A total of three thermal process sequences were considered, two of which included thermal soaks and one which was left in the as-cured condition. The thermal treatments were as shown in Table 4.1:

Table 4.1. Thermal Treatment of Composite Tensile Bars

	As-Cured	T.T.2	T.T.3
Thermal Treatment	No Thermal	190°C for 5 Hrs	190°C for 5 Hrs
	Treatment	68°C for 5 Hrs	57°C for 2 Hrs
		190°C for 5 Hrs	190°C for 5 Hrs
			190°C for 5 Hrs

The furnace temperature of the thermally-treated plates was monitored by inserting a thermocouple into the furnace. A data logger, which recorded and displayed the furnace temperature every ten minutes, provided a hardcopy of the composite plate thermal treatment. The equipment used for the thermal processing was a Thermcraft furnace, Model #218-18-24-BX-ATM. The processing consisted of placing the tensile bars in the furnace,

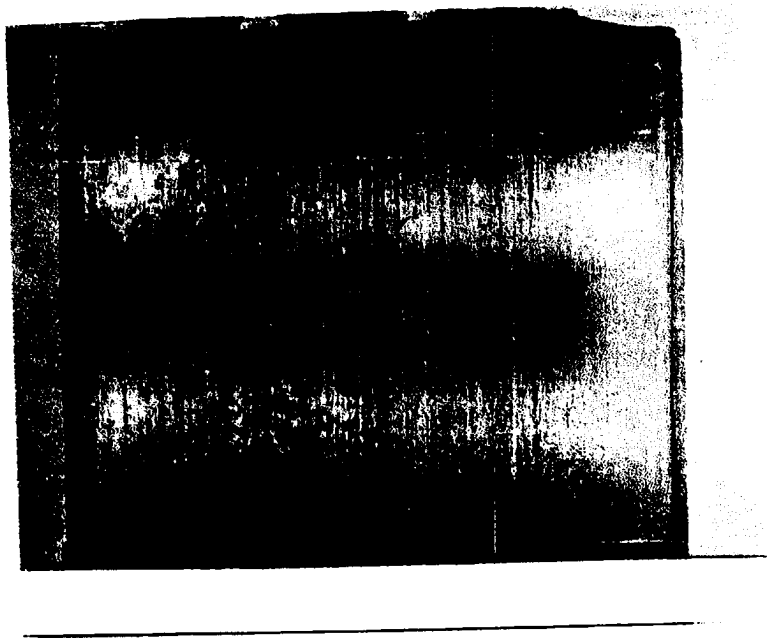

Figure 4.2 Overall view of As Cured composite plate. Laminate layup is comprised of 9 layers $[0_4,90_1,0_4]$.

ramping slowly to the desired temperature under atmospheric conditions, thermally conditioning the composite plates, ramping down to room temperature at a rate of ~5°C/min.

4.3 Composite Tensile Design

The composite tensile design was selected in accordance with ASTM D3039. The standard is based on the fiber type, fiber length, and testing direction. The recommended dimensions versus the actual dimensions are shown in Table 4.2 below. The designated values are based on longitudinally oriented, continuous, graphite fibers. All of the actual values are based on average measurements obtained from the tensile bars by the use of calipers.

Table 4.2. Dimensions of Tensile Specimens for Composite Material

	Recommended per ASTM 3039 (mm)	Actual (mm)
Tensile Specimen Thickness	0.508-2.54	1.02
Tensile Specimen Length	127 Minimum	228.6
Tensile Specimen Width	12.7	12.8

4.3.1 Tensile Bar Design for Testing Composite Specimens

Procedures that have been developed for tensile testing composite materials do not address some of the potential difficulties associated with specimen design and testing. ASTM Standard D3039 designates recommended widths, lengths, and thicknesses for tensile

testing both continuous and discontinuous fiber-reinforced composites. However, the standard does not address the subtleties, such as selection of appropriate specimen thickness to achieve ultimate failure stress, type of tab material utilized, or tab angle. The standards/procedures that have been developed for testing composite systems are too broad to encompass all composite materials. The problems encountered in obtaining valid data when tensile testing graphite bismaleimide suggest that additional design and testing criteria are necessary for developing a successful tensile test. However, the modifications introduced into the tensile specimens have resulted in more consistent data measurements. A number of factors must be considered when tensile testing graphite-reinforced, brittle polymeric materials, such as graphite bismaleimide (Gr/BMI). In particular, specimen shape, required thickness of tensile bars to cause fiber failure, importance of tabbing material and design, and material sensitivity to stress concentrations, induced by machining and extensometers, need to be studied in detail.

4.3.2 Specimen Shape

Prior to material fabrication, significant attention was given to specimen shape and thickness. Studies using finite element analysis (FEA) have been conducted by others, in order to observe the effects of contour radii on flat tensile specimens of advanced composites.[14] The premise for these studies was to generate a contour radius with the lowest stress values in the specimen transition zone, such that composite failure occurs within a specific region of the tensile bar. Although a contour radius reduces the chance of undesirable failure locations, the application is limited to composite systems that are typically ductile in nature. Due to the brittleness of the bismaleimide matrix material, contouring the specimen is ineffective due to shearing, which occurs along the transition region (contour radius) during the tensile test, thereby creating a straight-sided specimen. The macrographs shown in Figures 4.3 and 4.4, illustrate the actual tensile design that was used for testing purposes.

4.3.3 Specimen Thickness

The thickness of the tensile bar is critical for providing the type of fiber failure characteristics of graphite-reinforced composite systems, i.e., fiber explosion. Fiber explosion occurs due to the inability of a brittle material to undergo plastic deformation, hence resulting in multiple fracture sites. Based on the ASTM D3039 standard and composite layup orientation, a specimen thickness of 2.54 mm was selected. Tests using this thickness resulted in splitting caused by the compressive forces produced at the grips. Splitting is a type of shearing that occurs along the longitudinal direction of the tensile bar, resulting in an

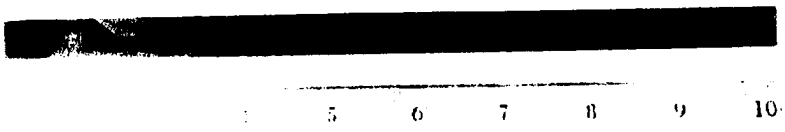

Figure 4.3 Overall view depicting water jet machined, tensile specimen - profile of width and length.

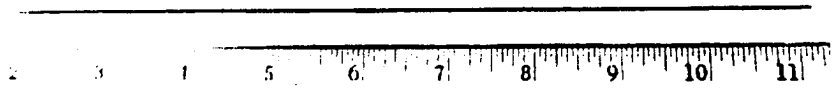

Figure 4.4 Overall view of water jet machined tensile specimen indicating thickness and length.

invalid test. The solution to this problem was to reduce the specimen thickness such that the specimen failed in the gage region rather than in the grips. The ASTM standard fails to consider the subtleties of a particular composite system. For example, the strength of graphite fibers is dependent on the processing techniques, i.e., Pitch-1550 MPa, PAN-2070-2760 MPa, or Rayon-2480-3100 MPa. Valid testing, which results in fiber failure near the center of the tensile bar, is highly dependent on the thickness of the specimen in order to cause failure in the desired location. Tensile testing Gr/BMI, utilizing a graphite fiber MR-56-2 as the reinforcement, which has a tensile strength of ~2400 MPa, requires a significantly reduced thickness (1.14 mm) in order to achieve fiber failure. Splitting, which is caused by exceeding the compressive strength of the material located at the grips, is a direct result of utilizing a thicker specimen, such that failure occurs by a crushing force caused by the wedge grips.

4.3.4 Tab Material Selection

The material used for tabbing the specimens can aid in reducing the likelihood of compressive failure at the grips. Tab material selection is based on the stiffness of the composite versus the stiffness of the tab material. Typically, the tab material should be less stiff than the test laminate as per MIL-HDBK-17B-1. Poisson's ratio, which is a measure of the ratio of strain in the longitudinal direction to the strain in the transverse direction, was utilized to determine an effective stiffness value for tab material selection. There exists a wide range of materials that are less stiff than Gr/BMI (lower Poisson's ratio), hence tab material selection encompasses nearly any material. However, based on experience, a material exhibiting a high Poisson's ratio will reduce the tendency for compressive failure at

the grips. Aluminum, which has a Poisson's ratio of 0.33, was determined to be the best candidate for tab material selection. The changes made in both specimen thickness and tab material selection increased the effectiveness of achieving a valid test.

4.3.5 Tab Angle for Tensile Bar

By utilizing high-speed video in order to observe the failure mode, i.e., failure locations, local stress concentrations induced by the tabs and extensometer were identified. Tab design was modified and the amount of pressure exerted by the extensometer knife edges was reduced, in an attempt to minimize the degree of damage in localized regions (i.e., tab/composite interface), where high stress concentrations were apparent. Two types of tab designs were used for the tensile tests (Figures 4.5 and 4.6). The tab contours included a 15° tab angle and a 50.8 cm radius. The tab variation was implemented in an effort to minimize the stress concentrations at the tab/composite interface.

4.3.6 Measurements Performed by Extensometer and/or Strain Gage

Strain measurements were difficult to obtain, due to either stress concentrations induced by the extensometer, or the loss of strain gages during fiber failure. By reducing the pressure induced by the knife edges, one can reduce the local stress concentration. The pressure was reduced by decreasing the number of rubber band windings, which held the extensometer to the tensile bar. Enough pressure had to be maintained in order to prevent the knife edges from slipping during the test.

A complete representation of the composite behavior was available by

Figure 4.5 Detailed view of tab design with a 15° angle.

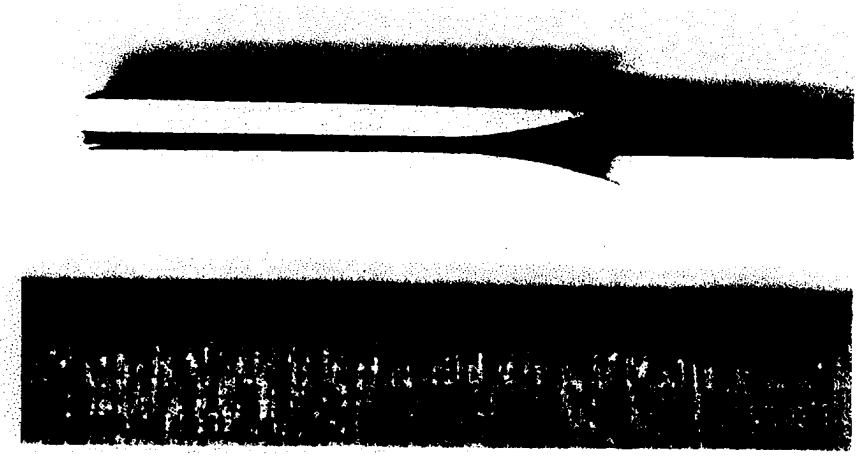

Figure 4.6 Detailed view of tab design with a 50.8cm radius.

combining both extensometer and strain gages. Strain gages helped generate a stress-strain curve that represented the actual strain behavior of the composite system, while minimizing fiber failure interference that commonly affects measurements obtained by extensometry.

4.4 Equipment Used for Tensile Testing Composite Material

The apparatus that was utilized for testing the composite specimens was an Instron, Model 1335 (Figure 4.7). Mechanical wedge grips were used to secure the specimen, as shown in Figure 4.8. The equipment, used for recording the data output from the tensile tests, included a Nicolet 310 oscilloscope (Figure 4.9) and the X-Y recorder connected to the Instron.

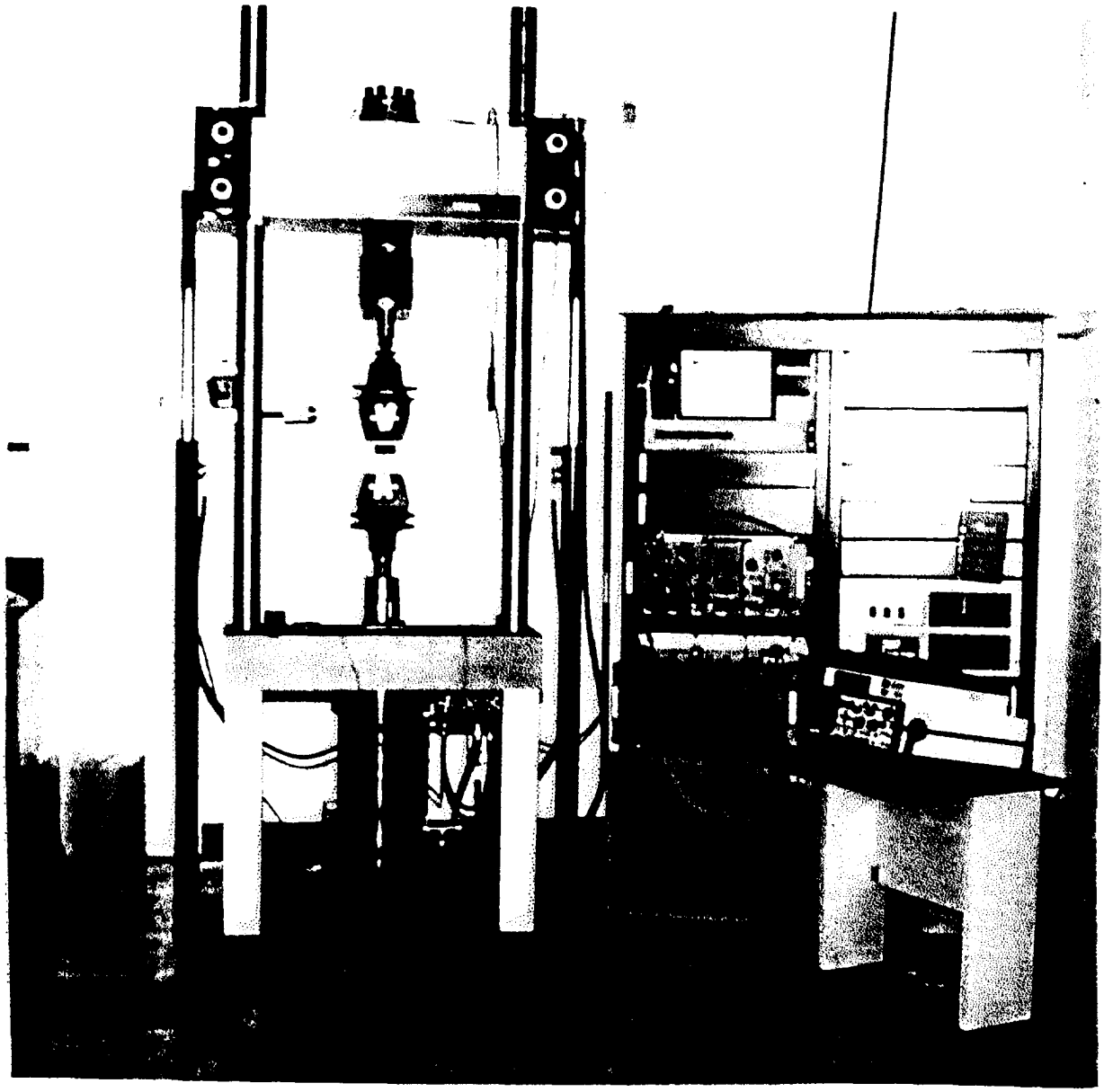

Figure 4.7 Instron, Model 1335 utilized for tensile testing composite samples.

Figure 4.8 Detailed view of test set-up depicting mechanical wedge grips (arrows) used for testing composite tensile specimens.

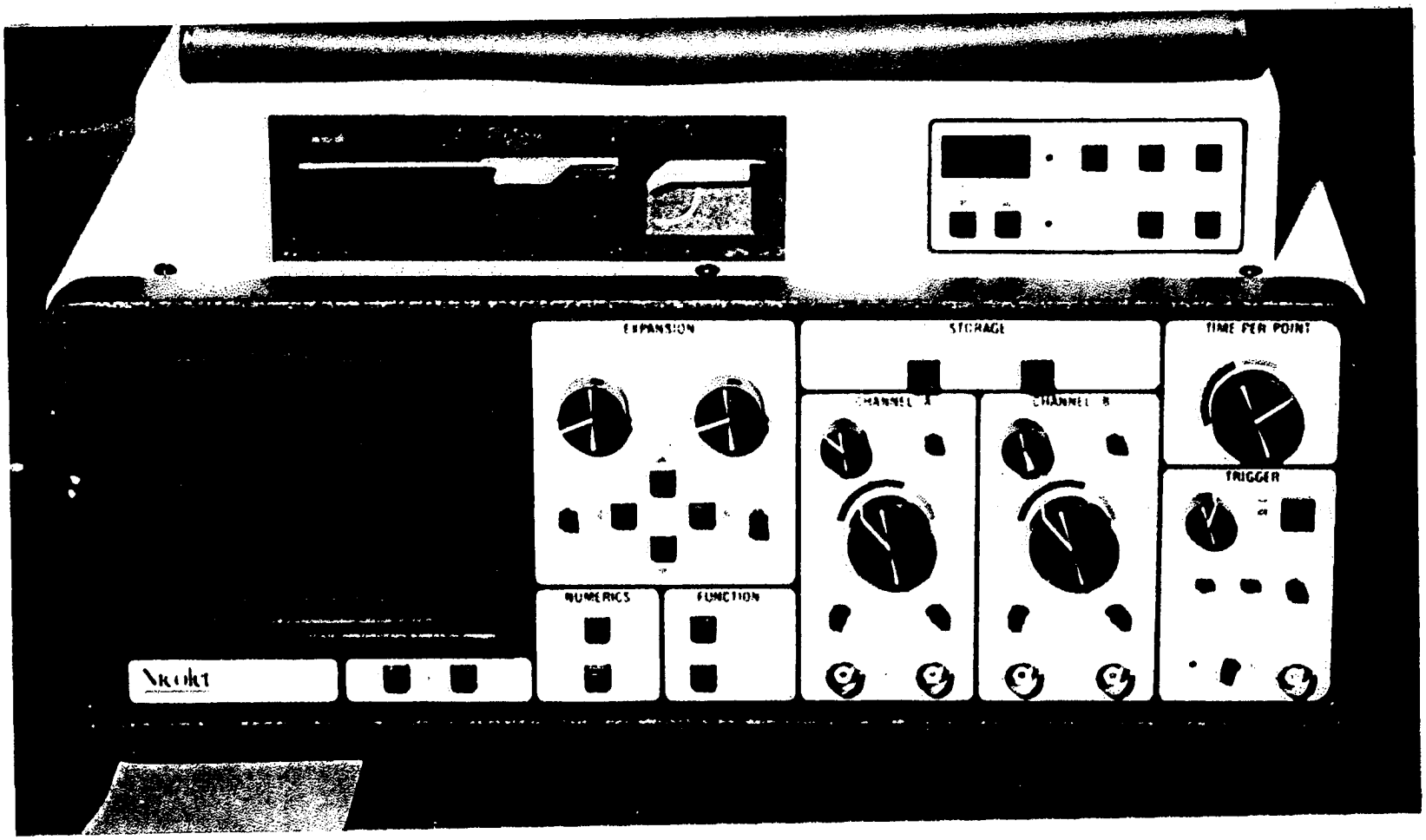

Figure 4.9 Overall view of Nicolet 310 oscilloscope utilized in recording data output from tensile tests.

4.5 Experimental Design

The test procedure was designed to encompass the effects of dynamic versus slow tensile testing, post-cure thermal treatments, and finally variation in tab angle. The experiment was conducted according to the chart shown in Table 4.3:

Table 4.3. Experimental Design for Testing Composite Specimens

Plate Number	Thermal Cycle*	Tab Orientation	Loading Rate (mm/sec)
1	As-Cured	15° Angle	0.22
1	As-Cured	15° Angle	121
2	As-Cured	50.8 cm Radius	0.22
2	As-Cured	50.8 cm Radius	121
3	T.T.2*	15° Angle	0.22
3	T.T.2*	15° Angle	121
4	T.T.2*	50.8 cm Radius	0.22
4	T.T.2*	50.8 cm Radius	121
5	T.T.3**	15° Angle	0.22
5	T.T.3**	15° Angle	121
6	T.T.3**	50.8 cm Radius	0.22
6	T.T.3**	50.8 cm Radius	121

* T.T.2 = two five-hour thermal treatments at 190°C + five hours at 68°C.
** T.T.3 = three five-hour thermal treatments at 190°C + one two-hour treatment at 57°C + one three-hour treatment at 68°C.

Note: A total of 3 to 5 tensile bars were tested for each 1 to 12 grouping.

A number of factors were considered when testing the composite specimens, i.e., time of day, temperature/humidity of room. Therefore, the testing sequence for the tensile bars was randomized in an effort to minimize the effects of external influences on the test results. As an example, both static and dynamic tests were run on the same day. In addition, samples representing all three heat treatments were selected for any single test date.

5.0 RESULTS

5.1 Overview of Test Results

Based on data consistency of the stress-to-failure values obtained from the tensile tests, in addition to the data comparisons supplied by the vendor, AMOCO, valid tensile tests were generated. The tensile bars of the valid tensile tests failed either in a characteristic "brooming" manner (Figure 5.1) or a combination of splitting and brooming (Figure 5.2). The tensile bars that did not produce valid test results, failed either due to splitting (Figure 5.3) or tab debonding (Figure 5.4), which occurred during the tensile test.

5.2 Linear Regression Model Utilized to Analyze Data

The test matrix, shown in Table 5.1, indicates the test results and test variables used in the data evaluation.

Table 5.1. Stress-to-Failure Results Obtained from Tensile Tests

	Tested at 0.22 mm/sec			Tested at 121 mm/sec		
	As-Cured	T.T.2*	T.T.3**	As-Cured	T.T.2*	T.T.3**
15° Angle	2243	2001	1863	2070	1760	1766
	2201	1808	1829	2174	1656	1656
	2291	1849	1849	1553	1608	2270
	1953					
50.8 cm	2070	1725	1622	2132	1656	1656
Radius	1697	1435	2270	1946	2270	1898
	1587		1849		1601	1898
	1918		1387		1387	
	1615					

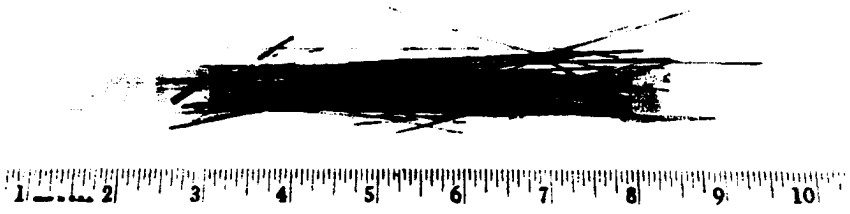

Figure 5.1 Overall view of failed tensile bar depicting "brooming" failure mode.

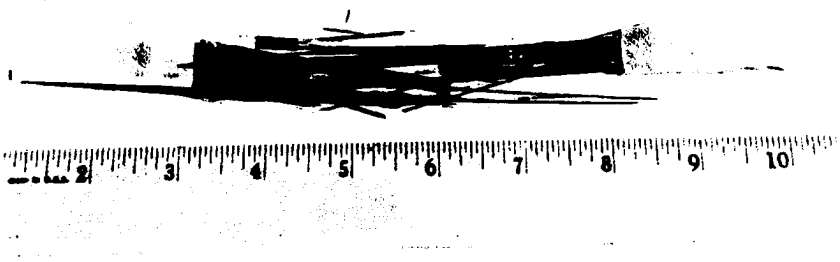

Figure 5.2 Overall view of failed tensile bar depicting "brooming" + splitting failure.

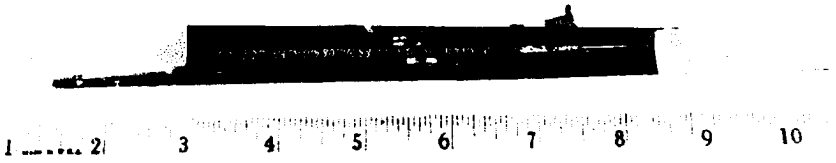

Figure 5.3 Overall view of failed tensile bar depicting splitting failure, resulting in invalid failure results.

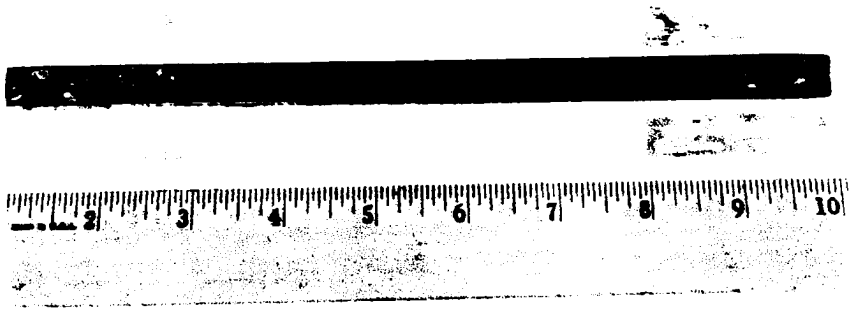

Figure 5.4 Overall view of failed tensile bar depicting tab debonding, which led to invalid failure results.

Bar graphs, identifying the interaction of these variables, were generated from the resulting stress-to-failure values. The predicted stress-to-failure values were obtained by applying a regression analysis via a computer program (Appendix A). The computer program was designed to consider variables, such as tab angle, testing rate, thermal cycling, strain-to-failure, failure mode - brooming or partial splitting + brooming, in order to provide a model that would determine whether an individual test condition had a dominant effect on the stress-to-failure results. The Beta values, that were generated by the model, were based on both a 90% and a 95% confidence level, which are shown in the output results of Table 5.2. The Beta terms (1 through 7) represent the conditions that were incorporated into the model, in order to generate the predicted values. The linear model was used in the form described below:

$$y = \beta_0 + \beta_1 x_1 + \beta_2 x_2 + \beta_3 x_3 + \beta_4 x_4 + \beta_5 x_5 + \beta_6 x_6 + \beta_7 x_7 + \epsilon$$

where x_1 = 1, if tested dynamically

= 0, if not

x_2 = 1, if tested at 50.8 cm radius

= 0, if not

x_3 = 1, if tested at Thermal Treatment 2

= 0, if not

x_4 = 1, if tested at Thermal Treatment 3

= 0, if not

x_5 = strain-to-failure value

x_6 = 1, if failed by brooming

= 0, if not (i.e., failed by splitting + brooming)

x_7 = -3, -2, -1, if plate #'s 1, 2, 3

= 1, 2, 3, if plate #'s 4, 5, 6

ϵ = error

The following data were taken from the output in Appendix B. Each Beta term is identified in Table 5.2 below.

Table 5.2. Beta Values and 90/95% Confidence Intervals from the Linear Regression Analysis

Term	Beta Value	90% Confidence Interval	95% Confidence Interval
$Beta_0$	1446.9		
$Beta_1$	54.6	±109	±131
$Beta_2$	-8.58	±122	±147
$Beta_3$	-105.5	±130	±157
$Beta_4$	-145.0	±121	±145
$Beta_5$	154.3	±181	±218
$Beta_6$	347.3	±137	±165
$Beta_7$	-31.5	±27	±33

The 90% confidence intervals for terms 4, 6, and 7 indicate that there exists a comparative significance on the variables that were considered. The Beta terms are represented by the following parameters:

β_1 - static or dynamic

β_2 - 50.8 cm radius/15° angle

β_3 - as-cured, Thermal Treatment 2

β_4 - Thermal Treatment 3

β_5 - stress-to-failure values

β_6 - failure mode

β_7 - composite plate number

The significance of the Beta terms and confidence levels will be identified in the Discussion section.

5.3 Analysis of Data Obtained from Tensile Tests

The stress-to-failure results were statistically evaluated in an effort to support the data trends that were analyzed using bar plots. This section describes the comparative results of the stress-to-failure values obtained from the tensile tests and the statistical model.

5.3.1 Static Tensile Test Utilizing 15° Tab Angle Comparing Thermal Treatments (as-cured, T.T.2, T.T.3)

The bar graph, shown in Figure 5.5, compares the average stress-to-failure values of tensile bars that were subjected to the three thermal conditions identified in Section 3.2. The bar plot indicates that there was a decrease in the average stress-to-failure values for the specimens that were subjected to Thermal Treatments 2 and 3. Specimens obtained from

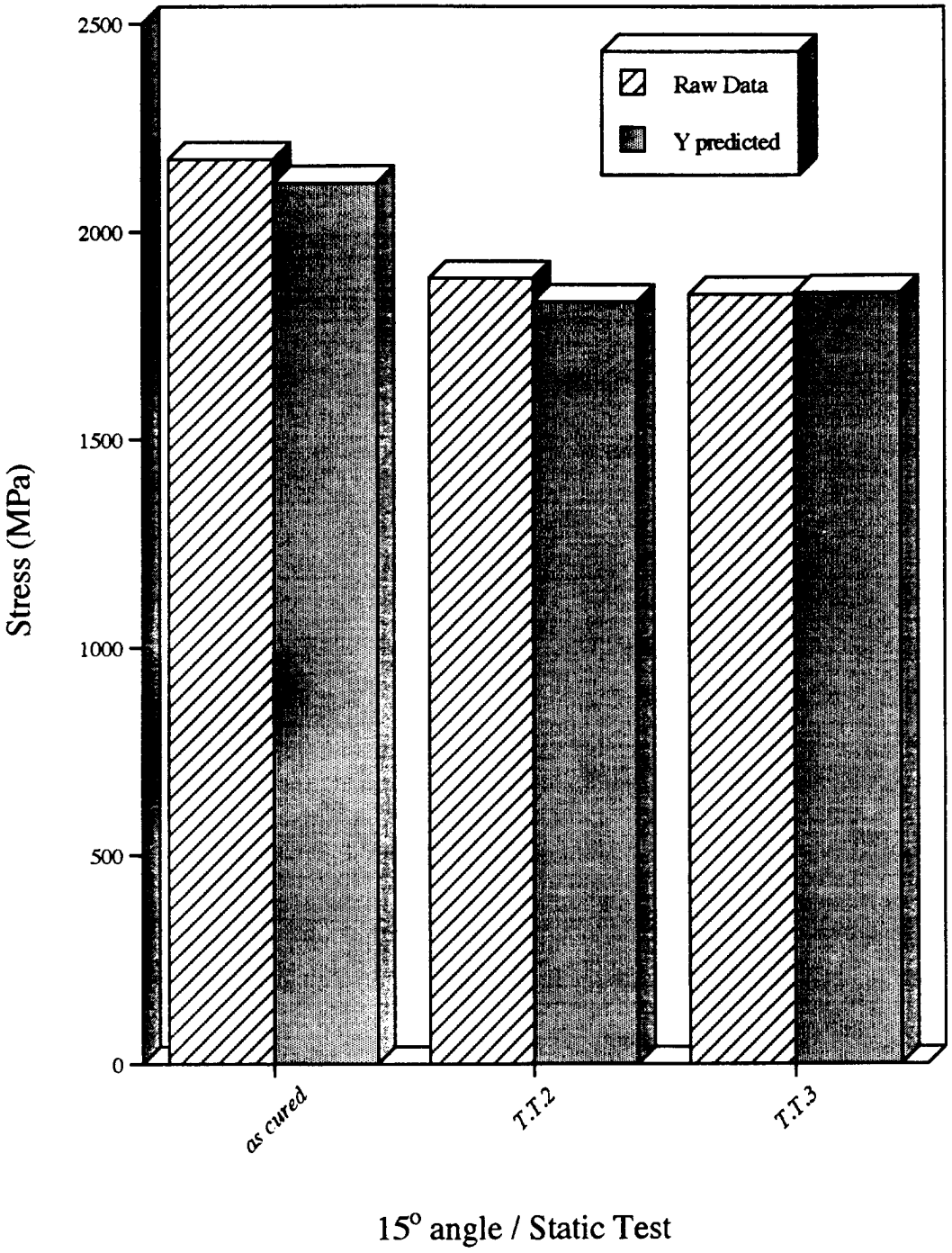

Figure 5.5 Static tensile tests with 15° tab angle comparing thermal treatments.

T.T.3, which underwent the greatest amount of thermal conditioning, exhibited a 19% reduction in stress-to-failure values. Specimens obtained from T.T.2 also revealed a 16% reduction in the stress-to-failure values. The reduction percentages were based on the as-cured condition, which was established as a baseline. Comparisons of the predicted values of Thermal Treatments 2 and 3 indicate that there was little difference in the average stress-to-failure values. Therefore, short-term thermal exposure effects (T.T.2 and T.T.3) had little influence on the stress-to-failure values.

5.3.2 Static Tensile Test Utilizing 50.8 cm Radius Tab Comparing Thermal Treatments (as-cured, T.T.2, T.T.3)

In an effort to reduce the stress concentration at the tab/composite interface, a 50.8 cm radius tab was employed. The tab design is discussed in Section 4.3.5. The comparison of thermal treatments is shown in the bar graph of Figure 5.6. The results indicate that there was a 12% reduction in the average stress-to-failure values of T.T.2. The raw data stress-to-failure values for T.T.3 were greater than the T.T.2 conditions. Comparing the results of the as-cured condition to those of T.T.3, a slight decrease in stress-to-failure values of T.T.3 was observed. The predicted stress-to-failure values for the as-cured condition were observed to be greater than those generated by the raw data. The predicted stress-to-failure data from Thermal Treatment 3 were found to be less than the raw data values. Thermal Treatment 2 indicated no significant variation between the two stress-to-failure values.

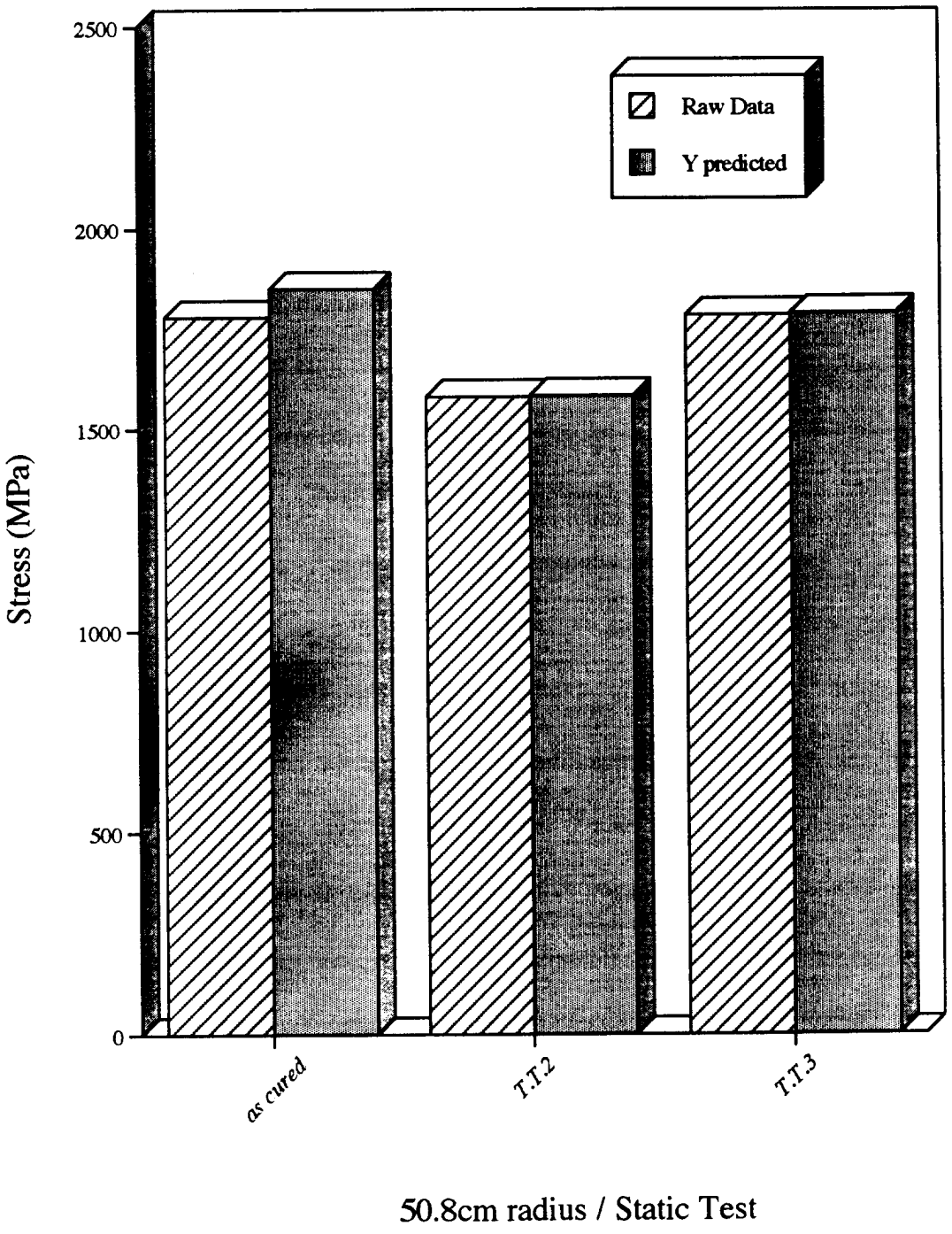

Figure 5.6 Static tensile tests with 50.8cm tab radius comparing thermal treatments.

5.3.3 Dynamic Tensile Test Utilizing 15° Tab Angle and Comparing Thermal Treatments (as-cured, T.T.2, T.T.3)

The bar graph, comparing the dynamic results of the three thermal treatments (Figure 5.7), indicates that the as-cured stress-to-failure values were higher than the values generated by the thermally-treated specimens. The predicted stress-to-failure value for the as-cured condition was greater than that which was generated by the raw data. The thermally-treated specimens, which had a greater number of microcracks due to the thermal exposure, resulted in lower stress-to-failure values. Again, the stress-to-failure values of T.T.3 were significantly greater than those of T.T.2. The predicted stress-to-failure values of the thermally-treated specimens were compared with the raw data values in order to determine if the difference was a result of the dynamic testing, or other variables, such as the tensile bar location on composite plate, failure mode, composite plate number from which the tensile bar was obtained. Thermal Treatments 2 and 3 exhibited very little variation in comparing the predicted values to the raw data. The data suggest that the tensile bars subjected to Thermal Treatment 3 had higher dynamic stress-to-failure values than Thermal Treatment 2, which may have resulted from the formation of fewer microcracks in the T.T.3 specimens during thermal exposure.

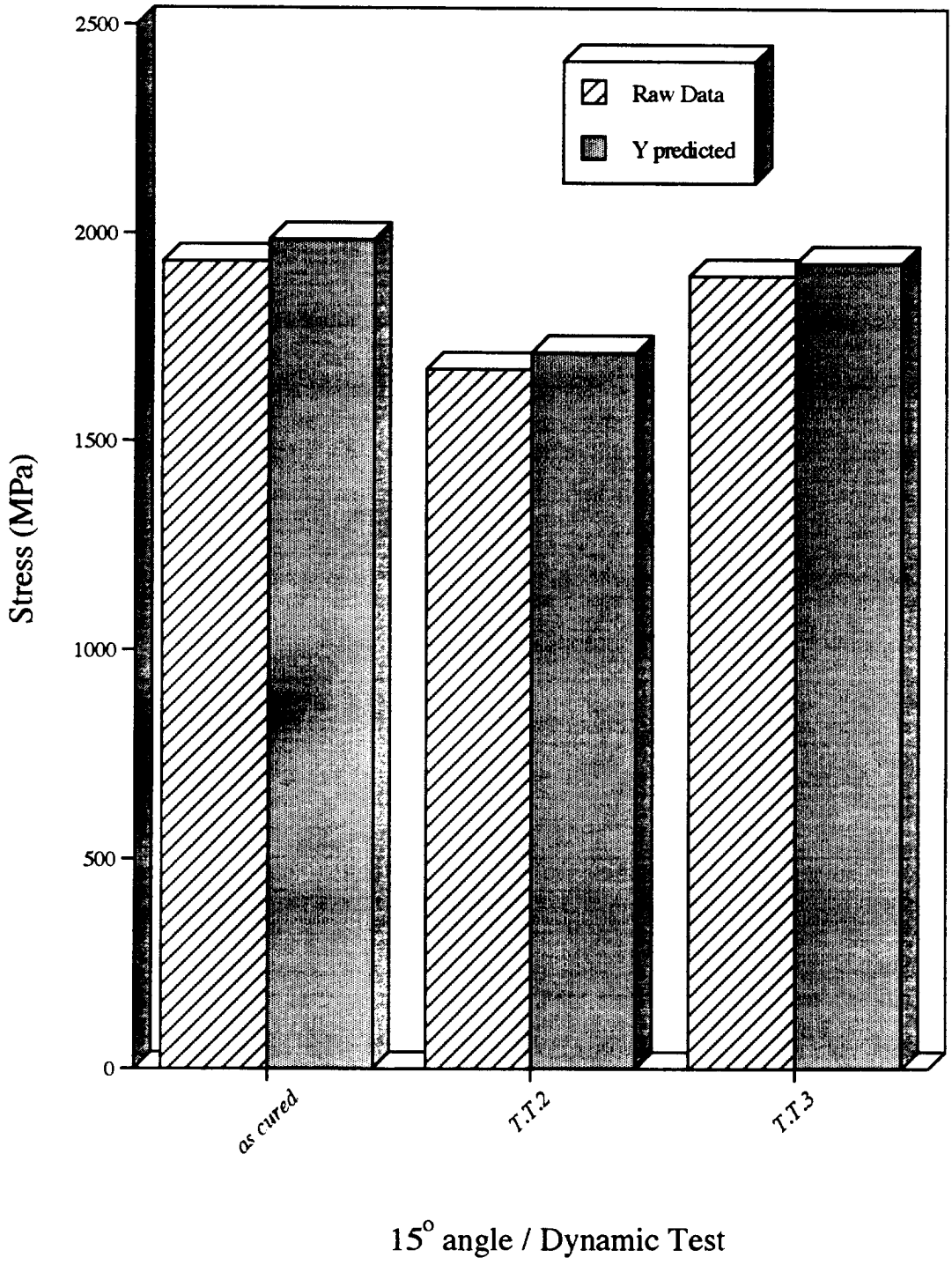

Figure 5.7 Dynamic tensile tests with 15° tab angle comparing thermal treatments.

5.3.4 Dynamic Tensile Test Utilizing 50.8 cm Radius Tab Comparing Thermal Treatments (as-cured, T.T.2, T.T.3)

The dynamic values of the three conditions, shown in Figure 5.8, indicate that there is approximately an 11% difference in the as-cured condition to that of Thermal Treatments 2 and 3. Thermal Treatments 2 and 3 do not show significant variation in the stress-to-failure results under dynamic conditions. The predicted values of all three conditions, obtained from the model, indicated an 8% decrease in the stress-to-failure values for the T.T.2 and T.T.3 conditions, as compared to the as-cured condition. The data indicate that the as-cured condition exhibited higher stress-to-failure results than the thermally-treated conditions. These results were consistent with the general trends observed throughout all of the tensile tests.

5.3.5 Static and Dynamic Comparisons of Tensile Bars with the 15° Tab Angle

The bar plot comparisons of the dynamic and static stress-to-failure values, shown in Figure 5.9, indicate that the tensile bars subjected to the static tests generated higher stress-to-failure values than those that were tested dynamically. There was a significant decrease in the as-cured condition of the dynamically tested tensile bars as compared to those subjected to static conditions. In comparing the static versus dynamic results of Thermal Treatments 2 and 3, there was little to no difference observed between the two test rates. There appeared to be a slight increase in the dynamically tested stress-to-failure values of

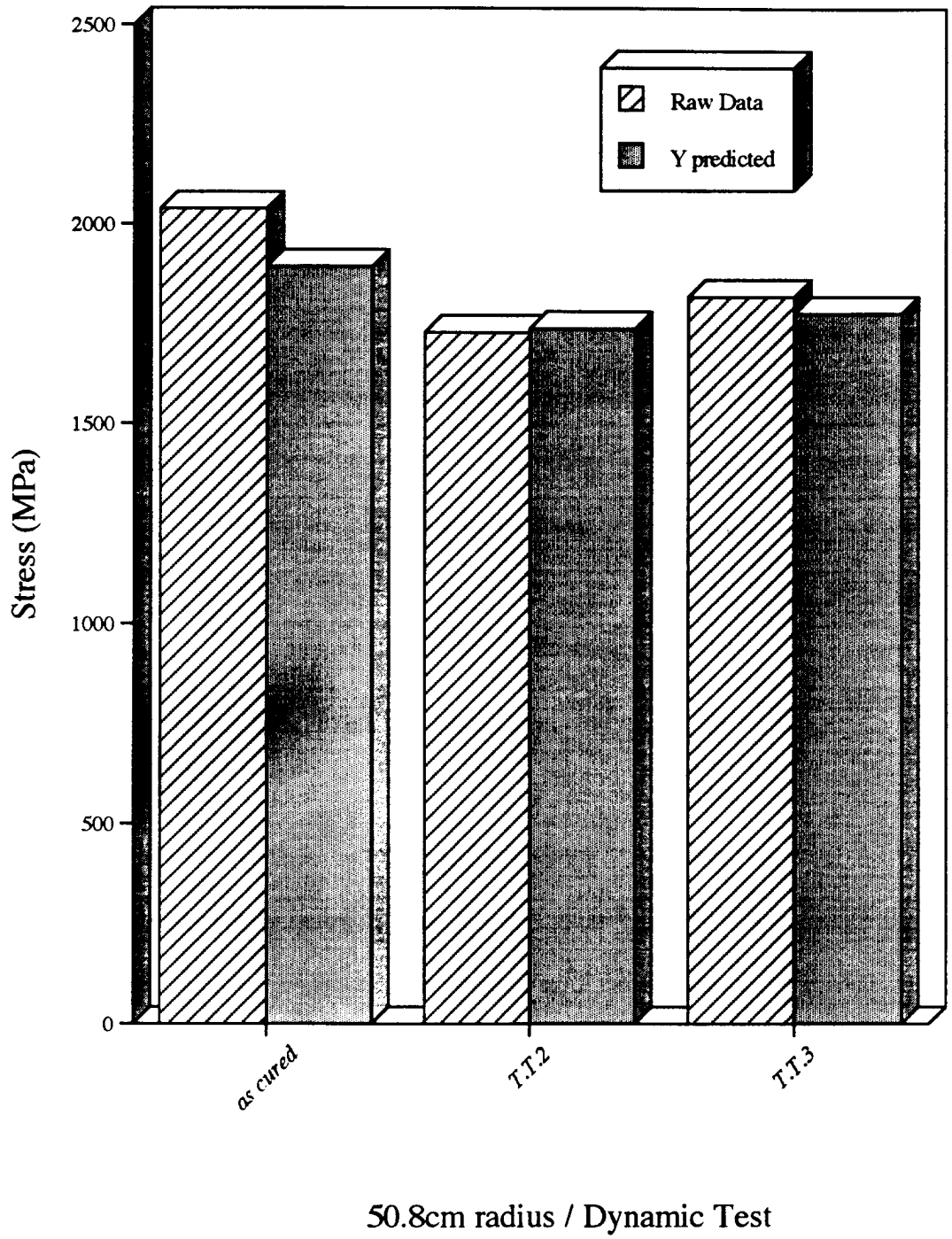

Figure 5.8 Dynamic tensile tests with 50.8cm tab radius comparing thermal treatments.

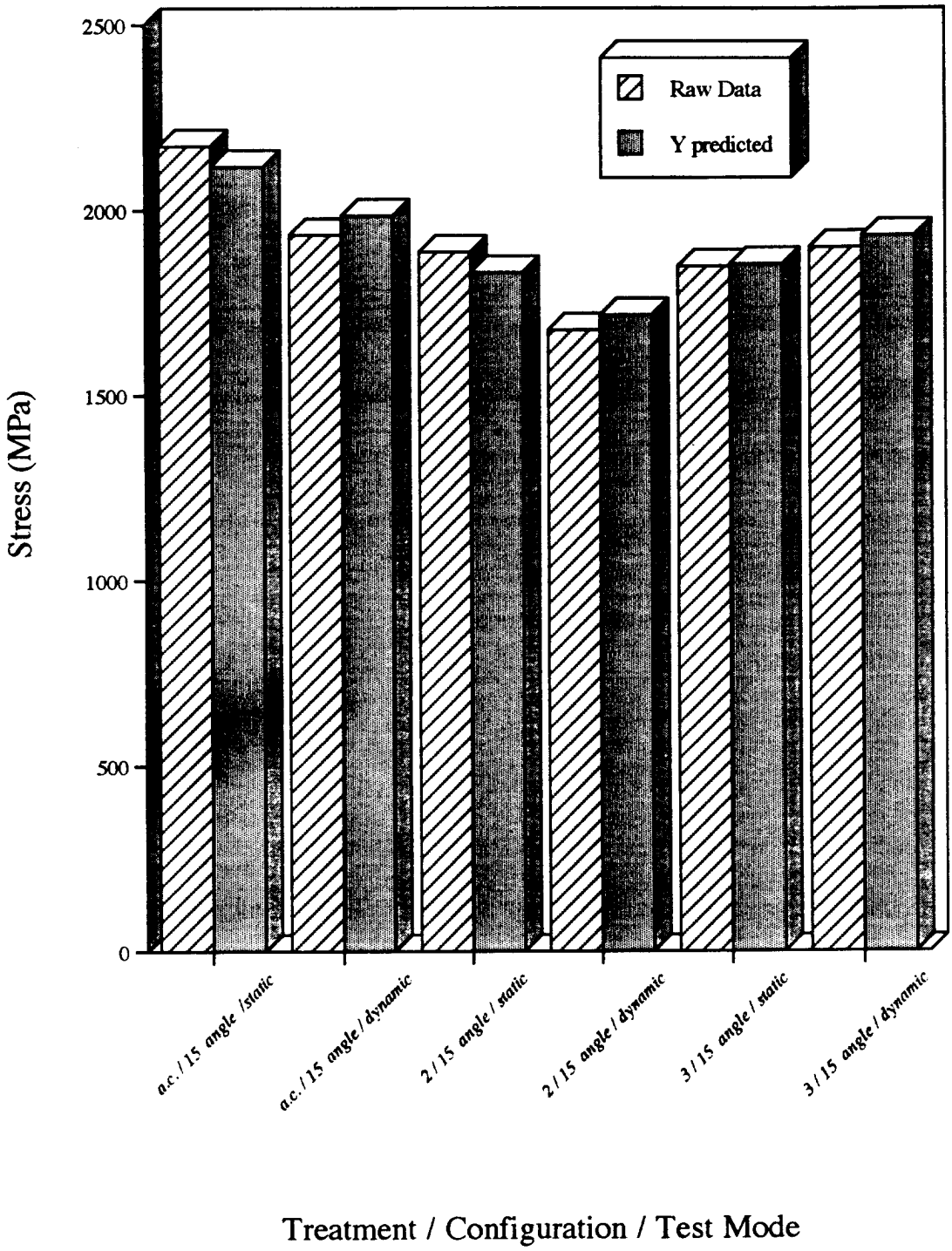

Figure 5.9 Static and dynamic comparisons of tensile bars with 15° tab angle.

T.T.3, as compared to the statically tested tensile bars with the same thermal treatment. However, the predicted values of the static and dynamic tests of T.T.3 indicate similar stress-to-failure results.

5.3.6 Static and Dynamic Comparisons of Tensile Bars with 50.8 cm Radius Tab

The static and dynamic comparisons of the tensile bars with the 50.8 cm radius tab (Figure 5.10) appear to indicate an increase in the stress-to-failure results of the dynamically tested bars of the as-cured and the T.T.2 conditions. Thermal Treatment 3 did not show any appreciable difference in the stress-to-failure results of the static and dynamic tests.

5.3.7 Comparisons of Tab Variation of Tensile Bars Subjected to Static Tensile Tests

The bar graph, shown in Figure 5.11, indicates that the raw data of the as-cured, Thermal Treatment 2, and Thermal Treatment 3 data exhibited a 25, 18, and 5% decrease, respectively, in the stress-to-failure values for the tensile bars with the 50.8 cm radius tabs, as compared to the resulting values of the bars equipped with the 15° tabs. The predicted values were consistent with the raw data trends in all three conditions shown.

5.3.8 Comparisons of Tab Variation of Tensile Bars Subjected to Dynamic Tensile Tests

The bar graph, shown in Figure 5.12, compares the effects of tab variation on the dynamically tested specimens. The samples subjected to the as-cured condition showed a 6% increase in the raw data test values for the specimens with the 50.8 cm radius tabs. The as-cured predicted values for the as-cured condition indicated that there was a decrease in the stress-to-failure results of the specimens that were tested with the 50.8 cm radius tabs. The T.T.2 data indicate that the tensile bars tested with the 50.8 cm radius tabs showed an 8% increase in the stress-to-failure values for the raw data. The predicted values for this thermal treatment showed a slight increase in the tensile bars tested with the 50.8 cm radius tabs. Thermal Treatment 3 indicated that there was a 7 and 8% decrease in the stress-to-failure values for the raw and predicted data, respectively.

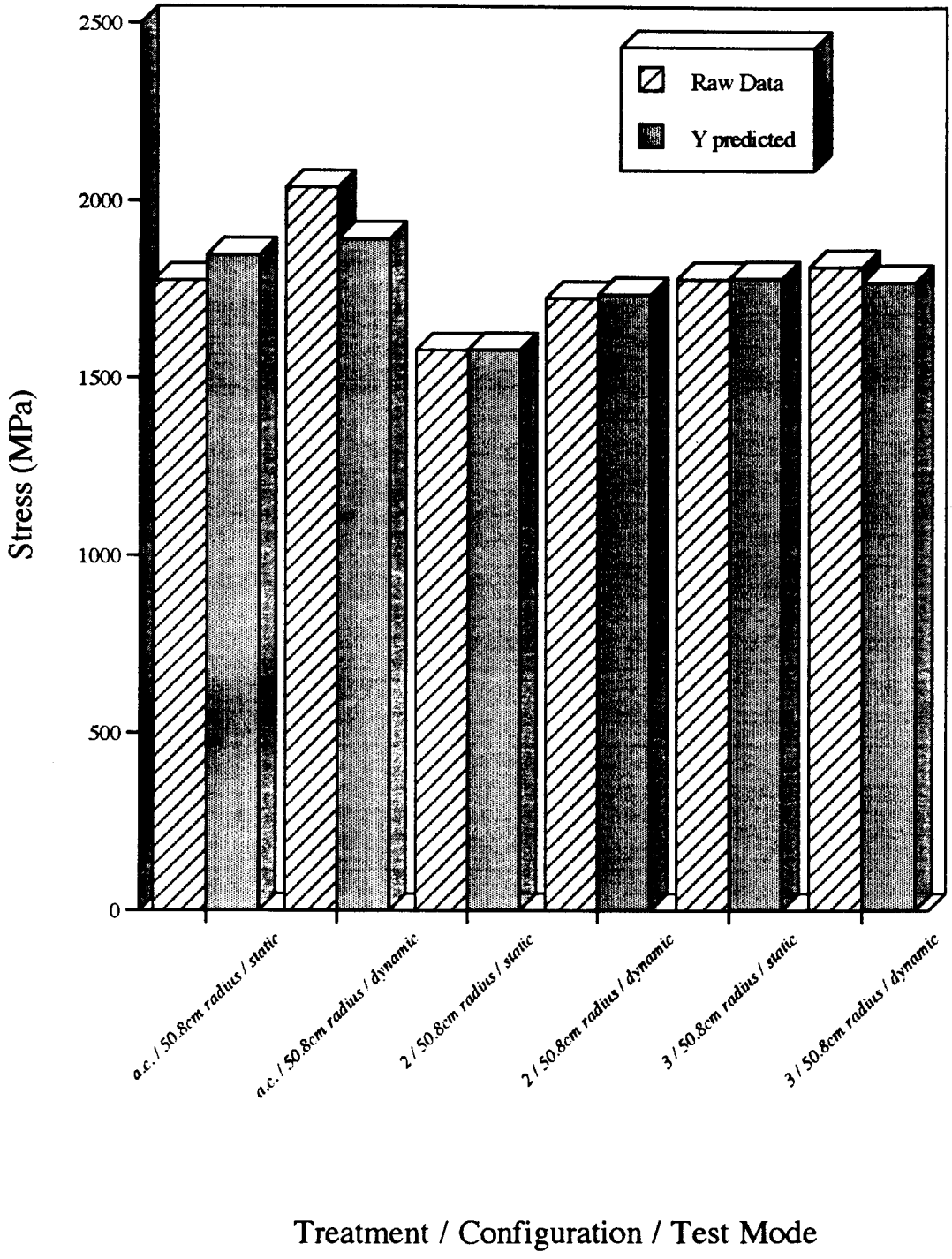

Figure 5.10 Static and dynamic comparisons of tensile bars with 50.8cm tab radius.

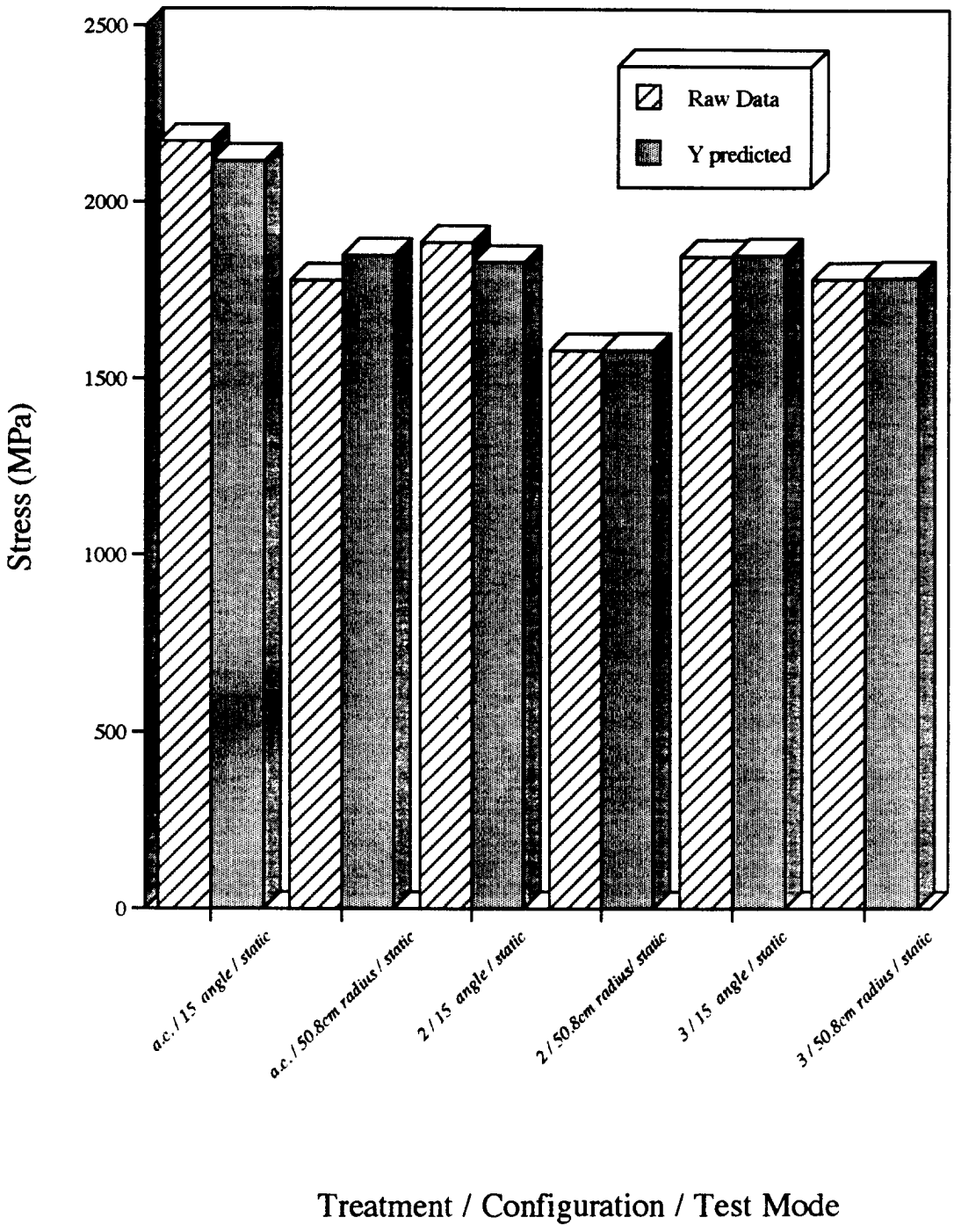

Figure 5.11 Comparison of tab variation of tensile bars subjected to static tensile tests.

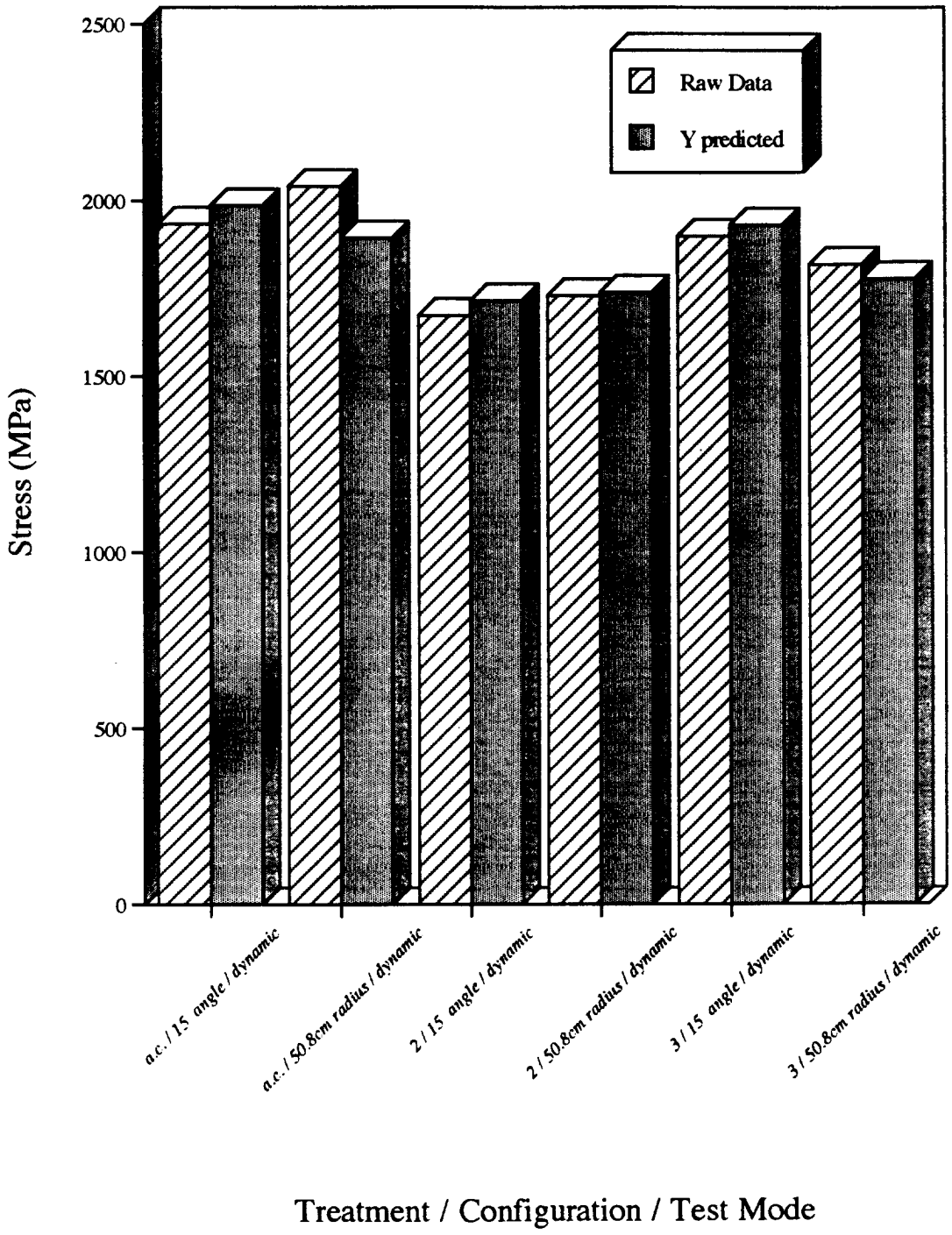

Figure 5.12 Comparison of tab variation of tensile bars subjected to dynamic tensile tests.

6.0 DISCUSSION

6.1 Development of the Tensile Bar Utilized for Testing

The thickness of the composite plates was developed according to ASTM 3039, which designates a range of 0.508 to 2.54 mm. Based on this range, composite plates with a thickness of 2.5 mm were fabricated. However, when the tensile bars were tested, splitting occurred in response to the force induced by the compressive pressure of the wedge grips. This type of failure was undesirable and as a result, new plates were fabricated with a reduced thickness. This new thickness was based on the cross-sectional area of the original specimens, away from the grips, that would cause failure prior to a compressive force failure. The resulting thickness value was determined to be 1.02 mm. Even with the new thickness, the tensile bars encountered some fiber crushing induced by the wedge grips. Localized fiber breakage occurred at the tab/composite edge interface, which caused premature failure. In an effort to circumvent this problem, a tab with a 50.8 cm radius was incorporated into the test parameters. Contouring the tabs reduced the propensity of fiber failure near the tab/composite interface. However, a small degree of fiber fracture near this interface still continued to occur throughout the tensile testing. The effect on the stress-to-failure values as a result of fiber fracture at the tab/composite interface was considered to be minimal.

6.2 Composite Failure Modes

Three distinct types of failure modes, as a result of the testing, were observed (i.e., brooming, splitting + brooming, and splitting). The general appearances of each of these modes of failure are shown in Figures 5.1, 5.2, and 5.3, respectively.

Brooming-type failures exhibited the highest stress-to-failure values and were therefore the most desirable of the three failure modes. The concept of failure by brooming is demonstrated by gradual fiber failure leading to final rupture.

Tensile bar failure, by splitting + brooming, resulted in lower stress-to-failure values than a brooming-type failure. This failure condition appeared to occur at the 0°/90° interface of the composite tensile bar. This type of delamination resulted in fibers breaking away in groups, as opposed to individual fiber rupture. The cracking, which occurred at the 0°/90° composite interface, was initiated at the edges of the test coupon, where fibers had been broken as a result of machining the tensile bar shape.

The most undesirable failure is caused by splitting, which does not generate valid test results. Splitting can be a function of bending, induced by improper placement of the tensile bar in the wedge grips of the test instrument, or by "bowing" in the width direction of the tensile bar.

The type of failure that was commonly observed in the "valid" tensile tests was identified as translaminar failure or brooming, which occurs as a result of fiber failure within a composite ply. Translaminar failure is exemplified by a fiber-dominated morphology, whereby failure occurs as a result of the formation of multiple crack zones, originating from a single source. The "source" or crack initiation origin, may be at the 0°/90° interface of the

tensile bar, where fiber/resin debonding extends across the ply thickness, thereby forming a crack.[3] It has been macroscopically observed[2] that composite failure involving translaminar tension fractures is characterized by numerous fibers projecting from the main fracture plane with little evidence of delamination.

6.3 Discussion of the Regression Analysis Performed on Raw Data

A computer program was written in order to evaluate the data generated from the tensile tests using regression analysis or the least squares method. This method determines the values of the constants in the chosen equation, that minimize the sum of the squared deviations of the observed values, from those predicted by the equation. The following assumptions were incorporated into the analysis:

- The experimental design was developed in a way as to provide typical data.
- Statistical independence: each response (y_i) is statistically-independent.
- The equation chosen is linear in the k independent variables and takes the form as described in Section 5.2.

The least squares method determines the values of the β_i's. Each β_i indicates the effect of that test condition on stress-to-failure. Additionally, the program computes the 90% and 95% confidence limits for each β_i. For example, if the confidence interval contains zero, the implication is, that particular test condition does not affect the stress-to-failure values. If it does not contain zero, that particular Beta value has a strong effect on the stress-to-failure

results. Based on the results generated from the computer output, β_i, for i = 4--thermal cycle 3, 6--failure mode, and 7--composite plate number, appear to have an influence on the resulting data.

Initially, variables 1 through 4 were included in the model. The Beta terms are identified by the statistical program as follows:

β_1 - static or dynamic

β_2 - 50.8 cm radius/15° angle

β_3 - as-cured, Thermal Treatment 2

β_4 - Thermal Treatment 3

β_5 - stress-to-failure values

β_6 - failure mode

β_7 - composite plate number

These variables alone were not sufficient to explain the variation in the stress-to-failure values. Therefore, variables 5 through 7 were incorporated into the model. As a result of introducing these additional variables, there was a considerable reduction in the variability in y, and a considerable increase in the correlation coefficient and square of the correlation coefficient, which are desired. The model appeared to predict values fairly well, with certain Beta terms affecting the stress-to-failure results.

6.4 Effects of Thermal Exposure on Graphite Bismaleimide

It was noted in the result section of 5.1.1, that a decrease in the average stress-to-failure was observed for the thermally-conditioned tensile bars. This reduction in strength

that was observed in the T.T.2 and T.T.3 conditions is associated with an increase in the degree of microcracking in the matrix as a result of the thermal treatments.[7]. Weakening of the brittle matrix, resulting in premature failure, may also have originated from inherent flaws within the material, i.e., fiber matrix debonding or matrix voiding. These conditions are exacerbated by temperature fluctuations and applied loading. Residual strains are magnified in cross-ply laminates, due to the expansion mismatch that occurs between the differing orientations. These strains, which are intensified by thermal exposure due to changes in the coefficient of thermal expansion (CTE), encourage the formation of microcracks within the composite laminate.[7] In addition to changes in the CTE, studies have shown that the fibers nearest to the external surface degrade as a result of thermo-oxidative effects caused by aging.[9] The results of T.T.2 and T.T.3 samples indicated a significant decrease in the stress-to-failure as compared to the as-cured condition. However, only slight differences in stress to failure values were observed when comparing the two thermally-treated conditions. It has been observed that higher temperatures for longer time periods (10,000 hours) increase the number of microcracks formed within the composite.[12] Although the T.T.3 condition was exposed for a longer time duration, the degree of microcracking appeared to remain constant. A possible explanation may be that the time duration of thermal exposure was not significant enough in order to increase the number of microcracks formed. The results suggest that, at this temperature, the number of microcracks formed achieves a "threshold" value, irrespective of the exposure time used in the experiment. Experiments have shown that long exposure

times at elevated temperatures (25,000 hours at 273°C) have caused matrix degradation to occur.[12] Therefore, longer thermal exposure times and higher temperatures may increase the number of microcracks generated in the composite samples.

6.5 Effects of Variation in Loading Rates on Graphite Bismaleimide

Dynamic testing of the tensile bars with the 15° tab angles did not exhibit significant variation in the stress-to-failure results, when comparing the resulting values to the static tests. The observed trends showed a slight decrease in the stress-to-failure of the dynamically tested samples. Studies on the effects of dynamic loading rates have been made on selected composite systems with varying layup orientations. According to the studies, no significant variation in dynamic strength was observed, when measured against the statically tested samples. However, on transversely-oriented samples, an increase in the transverse tensile strength occurred, as compared to the static counterparts.[5, 6] The graphite bismaleimide plates, that were fabricated for tensile testing, consisted of nine layers, eight layers in the 0° direction and one layer in the 90° direction. The 90° layer was positioned along the axis of symmetry. The variation in stress-to-failure values, comparing static to dynamic tests, may have been manifested within the 0°/90° interface, which acts as a weak link in the composite test specimen. The weakness at this interface may be caused by a number of factors, such as the difference in the coefficient of thermal expansion in the transverse and longitudinal directions, debonding at the 0°/90° interface and microcracking induced by the variation in the strain-to-failure values in the transverse and longitudinal directions.

6.6 Comparison of Tab Variation on Stress-to-Failure Results

Failure at the tab/composite interface, which leads to lower than predicted failure values, is a common occurrence when tensile testing composite samples. A uniform stress distribution along the tab surface is extremely important, in order to generate valid test results. Efforts to reduce the stress concentration at the tab/composite interface can be achieved by reducing the tab angle, while still maintaining enough surface area for gripping the specimen. ASTM 3039 recommends a tab angle equal to or greater than 5°. In order to retain a sufficient surface area to grip the tabs, 15° tab angles and a 50.8 cm radius were selected for a two-inch tab length. The 50.8 cm radius tab design resulted in reduced stress-to-failure values as compared to the 15° tab angle design. In addition, the comparative results of the tensile bars tested with the 50.8 cm radius tabs, did not generate the trends that were observed with the 15° tab angles. The effect of the 50.8 cm radius was correlated to the Beta values/confidence intervals obtained from the linear regression model. The model indicates that the Beta value for the 50.8 cm radius (β_2), caused a decrease of 51 MPa in the stress-to-failure results. The confidence interval for this Beta value was extremely high, which implies that the overall effect of the 50.8 cm radius tabs was insignificant. However, the bar charts indicate that the stress-to-failure values are lower and the comparative differences in test conditions are not as definitive as the stress-to-failure values recorded from the 15° tabbed specimens. The tab/composite interface of the tensile bars with the 50.8 cm radius tabs had a reduced surface area where the tab and composite were joined. This is an effect of the contouring of the tab radius. The location, where the tab contour begins, may have resulted

in a localized stress riser, due to the concept that contouring no longer plays a role in distribution of stress along the radius, hence causing fibers to fail along the tab/composite interface.

7.0 SUMMARY AND CONCLUSIONS

1. A successful technique for tensile testing polymeric composites has been developed. It was observed that by utilizing a straight-sided tensile specimen, using an appropriate specimen thickness for generating valid stress-to-failure results, carefully fixturing the composite specimens in the wedge grips, and using 15° tab angles, reliable test data were generated.

2. A computer program, designed to perform a statistical analysis, was developed in an effort to identify the primary influences that significantly affected the stress-to-failure results. The statistical analysis was incorporated into this work in order to provide a probabilistic mathematical model that would describe the relationship between y (stress-to-failure values) and x (test conditions). In addition, the program performed a linear regression analysis, which was utilized for identifying the test variables that influenced the stress-to-failure results. From the model, in conjunction with the actual data values, it was determined that thermal treatment, failure mode, and composite plate number, where samples were obtained, were the primary variables that significantly influenced the outcome of the test results. The highest stress-to-failure values were obtained from the as-cured condition, the tensile bar being obtained from the central location of composite plate, and failures that resulted in "brooming."

3. The analysis indicated that tab angle is an important factor to consider when testing composite materials. The tensile bars with the 50.8 cm radius tabs, did not reveal discernible trends in the resulting data. However, the tensile bars equipped with the 15° tab angles identified the effects of thermal treatment and loading rates.

4. It was observed, via results from tensile test data, that exposure to thermal processing decreased the stress-to-failure values. It has been suggested that this is related to residual stresses generated by the thermal exposure.

5. The stress-to-failure data trends are consistent with the hypothesis that increasing the thermal exposure increases the degree of microcracking and debonding located primarily at the 0°/90° interface. Tensile failure of the composite samples appeared to be localized at or near this interface.

6. Consistent with previous studies, stress-to-failure values from tensile bars subjected to various thermal exposures were found to be independent of effects associated with dynamic testing, as compared to their statically tested counterparts.

7. The findings of this experiment provide an important basis for PMC-related material selection criteria, in regard to future component design work, which incorporates thermal exposure in conjunction with dynamic loading rates.

8.0 FUTURE WORK

A number of areas may benefit from further research. The work performed in this study revealed the necessity for developing appropriate test procedures for a particular composite system. In order to generate reliable, consistent data, studies regarding optimum tensile design and testing for other composite systems should be considered.

Additional work involving mechanical testing at elevated temperatures and various loading rates would be beneficial in determining the effects of composite response to certain component applications.

There exists a need to evaluate and compare the effects of a toughened graphite bismaleimide system to that of an untoughened graphite bismaleimide composite. It would be interesting to observe if the toughening agents added to the new system increase the stress-to-failure values of thermally-treated specimens, as a result of decreasing the propensity for microcracking.

REFERENCES

1. B. Agarwal and L. Broutman, *Analysis and Performance of Fiber Composites*, John Wiley and Sons, 1990, pp. 21-23.

2. B. Smith, "Fractography for Continuous Fiber Composites," *Composites*, Vol. 1, 1987, pp. 786-793.

3. R.P. Harrison and M.G. Bader, "Damage Development in CFRP Laminates Under Monotonic and Cyclic Stressing," *Fiber Science and Technology*, Vol. 18, 1983, pp. 163-180.

4. D.R. Mulville and I. Wolock, "Failure of Polymer Composites," *Journal: Dev. Poly. Frac.*, Vol. 1, 1979, pp. 263-316.

5. I.M. Daniel, W.G. Hamilton, and R.H. LaBedz, "Strain Rate Characterization of Unidirectional Graphite/Epoxy Composite," *ASTM STP 787*, 1982, pp. 393-413.

6. Y.V. Suvorova, T.G. Sorina, I.V. Viktorova, and V.V. Mikhailov, "Effect of Rate Loading on the Type of Failure of Carbon Reinforced Plastics," *Russian Translation*, No. 5, 1980, pp. 847-851.

7. M. Simpson, P.M. Jacobs, and F.R. Jones, "Generation of Thermal Strains in Carbon Fiber Reinforced Bismaleimide (PMR-15) Composites - Part 1," *Composites*, Vol. 22, No. 2, 1991. pp. 89-97.

8. K.K. Chawla, *Composite Materials*, Springer-Verlag, NY, 1987, pp. 189-191.

9. D. Scola, "Thermo-Oxidative Stability of Graphite Fiber/PMR-15 Polyimide Composites at 350°C," *High Temperature Polymer Matrix Composites*, Noyes Data Corporation, NJ, 1987, pp. 214-244.

10. F.J. Magendie and J.C. Seferis, "Thermal Stability of Ceramic and Carbon Fiber Reinforced BMI Matrix Composites," *SAMPE*, 1990, pp. 2280-2288.

11. K.J. Bowles and G. Nowak, "Thermo-Oxidative Stability Studies of Celion 6000/PMR-15 Unidirectional Composites, PMR-15 and Celion 6000 Fiber," *Journal of Composite Materials*, Vol. 22, 1988, pp. 966-985.

12. J.F. Haskins and J.R. Kerr, "Effects of Real-Time Thermal Aging on Graphite/Polyimide Composites," *High Temperature Polymer Matrix Composites*, Noyes Data Corporation, NJ, 1987, pp. 309-313.

13. M.P. Hanson and T.T. Serfini, "Surface Protection of Graphite Fabric/PMR-15 Composites Subjected to Thermal Oxidation," *High Temperature Polymer Matrix Composites*, Noyes Data Corporation, NJ, 1987, pp. 282-286.

14. Jeff A. Kessler and Donald F. Adams, "Composite Specimen Design Analysis. Vol. II: Experimental Effects," University of Wyoming, Jan. 1991, pp. 51-58.

15. William Mendenhall, *Introduction to Linear Models and The Design and Analysis of Experiments*, Wadsworth Publishing Company, Belmont, CA, 1968, pp. 26-46.

APPENDIX A

Basic A Program for Regression Analysis

```
10 MULTIPLE REGRESSION.
20  DIM X(100,10), XTRAN(10,100),Y(100),PI(10,10),XYPRD(10),B(10),P(10,10)
30  DIM AUG(10,20),AI(10,10),T95(50),T90(50)
40 FOR I=1 TO 50:READ T95(I):NEXT I
45 FOR I=1 TO 50: READ T90 (I):NEXT I
50 CLS:READ T$
60 PRINT T$: PRINT
70 READ N, NV
80 KK=1
90 FOR I=1 TO N
100  X(I,1)=1
110 READ Y(I):FOR J=2 TO NV:READ X(I,J);:NEXT J
130  GOSUB 1410
140 PRINT
150 NEXT I
160 NV=NV
170 FOR I=1 TO NV
180 FOR J=1 TO N:  XTRAN(I,J)=X(J,I): NEXT J
190 NEXT I
210 FOR I=1 TO NV
220 FOR K=1 TO NV
230  P(I,K) = 0!
240 FOR J=1 TO N: P(I,K)=XTRAN(I,J)*X(J,K)+P(I,K) : NEXT J
250 NEXT K
260 NEXT I
270  GOSUB 920
330 PRINT:GOSUB 1410:PRINT "DETERMINANT =";GOSUB 1410
350 FOR I=1 TO NV
360 XYPRD (I) = 0
370 FOR J=1 TO N:XYPRD(I) = X(J,I)*Y(J)+XYPRD(I):NEXT J
380 NEXT I
390 SUMY=XYPRD(1)
400 SSBO = SUMY*SUMY/N
420 FOR I=1 TO NV
430 B(I) = 0
440 FOR J=1 TO NV:B(I) = B(I)+PI(I,J)*XYPRD(J):NEXT J
450 NEXT I
460 PRINT:GOSUB 1410:PRINT "TERM              COEFF":GOSUB 1410
470 FOR I=1 TO NV
480 IM1 = I - 1
490  PRINT IM1, B(I):GOSUB 1410
500 NEXT I
510 BXY=0
520 FOR I=1 TO NV:BXY = B(I)*XYPRD(I)+BXY:NEXT I
530 SSRBO = BXY - SSBO
540  SUMY2 = 0
550 FOR J=1 TO N:SUMY2 = Y(J)*Y(J)+SUMY2:NEXT J
560 SSAR = SUMY2 - BXY
570 RSQ = SSRBO/(SUMY2-SSBO)
580 KK=KK+1
590 IF KK MOD 20 <> 0 THEN GOTO 580
600  GOSUB 1410
650 NMM=N - NV
660 PRINT: PRINT "ERROR VARIANCE = ",SSAR/NMM:"WITH  ";NMM;" D.F."
670 PRINT: PRINT " ERROR STANDARD DEVIATION =  ",SQR(SSAR/NMM)
```

```
680 PRINT:PRINT "R-SQUARED = "RSQ
690 PRINT:PRINT "CORRELATION COEFFICIENT = ", SQR(RSQ)
700 PRINT:PRINT "TERM                                        95% C.I.  90% C.I.
710 GOSUB 1410
720 SIGMA=SQR(SSAR/NMM)
730 FOR I=2 TO NV
740 FAC95=T95 (NMM)*SIGMA*SQR(PI(I,I))
745 FAC90=T90 (NMM)*SIGMA*SQR(PI(I,I))
750 PRINT I-1,B(I),"+/-";FAC95,FAC90:GOSUB 1410
760 NEXT I
770 PRINT:PRINT "WHAT NEXT? (1=STOP,2=SUMMARY,3=READ MORE DATA)"
780 INPUT MORE
790 ON MORE GOTO 910,800,50
800 CLS:KK=1
810 PRINT T$
820 PRINT: PRINT "    Y              YPRED          DIFF          %DIFF"
830 FOR I=1 TO N
840 YPRED = B(1)
850 FOR J=2 TO NV:YPRED = YPRED + B(J)*X(I,J): NEXT J
860 DIF = Y(I) - YPRED
870 PCDIF = DIF/Y(I)*100
880 PRINT Y(I), YPRED, DIF, PCDIF:GOSUB 1410
890 NEXT I
900 GOTO 770
910 END
920 M=2*NV
930 FOR I=1 TO NV
940 FOR J=1 TO M
950 IF J>NV GOTO 980
960 AUG(I,J) = P(I,J)
970 GOTO 1020
980 IF J-NV-I=0 GOTO 1010
990 AUG(I,J)=0
1000 GOTO 1020
1010 AUG(I,J)=0
1020 NEXT J
1030 NEXT I
1040 IEFF=0
1050 L=1
1060 D=1
1070 FOR ID=1 TO NV
1080 AMAX=AUG(ID,ID)
1090 MAX = ID
1100 FOR I=ID TO NV
1110 IF (ABS(AUG(I,ID))-(ABS(AMAX))<=0) GOTO 1140
1120 AMAX=AUG(I,ID)
1130 MAX=I
1140 NEXT I
1150 IF (ABS(AMAX)-10^-10<=0) GOTO 1380
1160 FOR J=ID TO M
1170 TEMP = AUG(ID,J)
1180 AUG(ID,J)=AUG(MAX,J)
1190 AUG(MAX,J)=TEMP
1200 NEXT J
1210 FOR I=1 TO NV
1220 IF (I-ID=0) GOTO 1270
1230 AIID=AUG(I,ID)
1240 FOR J=ID TO M
1250 AUG(I,J)=AUG(I,J)-AIID/AUG(ID,ID)*AUG(ID,J)
1260 NEXT J
```

```
1270 NEXT I
1280 NEXT ID
1290 FOR I=1 TO NV:D=AUG(I,I)*D:NEXT I
1300 D=ABS (D)
1310 FOR I=1 TO NV
1320 FOR J=1 TO NV:L=NV+J:AUG(I,L)=AUG(I,L,)/AUG(I,I):NEXT J
1330 NEXT I
1340 FOR I=1 TO NV
1350 FOR J=1 TO NV:L=NV+J:PI(I,J)=AUG(I,L):NEXT J
1360 NEXT I
1370 RETURN
1380 IERR = 1
1390 D=0
1400 RETURN
1410 IF KK MOD 20<>0 THEN GOTO 1470
1440 A$=INKEY$: IF A$=" " GOTO 1440
1450 CLS
1470 KK=KK+1
1480 RETURN
5000 REM THE 10 DATA LINES BELOW ARE 0.025 t VALUES FOR UP TO 50 d.f.
5010   DATA  12.7062,4.3027,3.181=24,2.7764,2.5706
5020   DATA  2.4469,2.3646,  2.3060,2.2622,2.2281
5030   DATA  2.2010,2.1788,2.1604,2.1448,2.1315
5040   DATA  2.1199,2.1098,2.1009,2.0930,2.0860
5050   DATA  2.0796,2.0739,2.0687,2.0639,2.0595
5060   DATA  2.0555,2.0518,2.4084,2.0452,2.0423
5070   DATA  2.0395,2.0369,2.0345,2.0322,2.0301
5080   DATA  2.0281,2.0262,2.0244,2.0227,2.0211
5090   DATA  2.0195,2.0181,2.0167,2.0154,2.0141
5100   DATA  2.0129,2.0117,2.0106,2.0096,2.0086
5105 REM THE 10 DATA LINES BELOW ARE 0.05 t VALUES FOR UP TO 50 d.f.
5110   DATA  6.3138,2.920,2.3534,2.1318,2.0150
5120   DATA  1.9432,1.8946,1.8595,1.8331,1.8125
5130   DATA  1.7959,1.7823,1.7709,1.7613,1.7531
5140   DATA  1.7459,1.7396,1.7341,1.7291,1.7531
5150   DATA  1.7207,1.7171,1.7139,1.7109,1.7081
5160   DATA  1.7056,1.7033,1.7011,1.6991,1.6973
5170   DATA  1.6955,1.6939,1.6924,1.6909,1.6896
5180   DATA  1.6883,1.6871,1.6860,1.6849,1.6839
5190   DATA  1.6829,1.6820,1.6811,1.6802,1.6794
5200   DATA  1.6787,1.6779,1.6772,1.6766,1.6759
6000 DATA RUN OF 10/20/94 (STRESS TO FAILURE (MSI))
6010 DATA 38,7
6020   DATA  2243,0,0,0,0,1,-3,2201,0,0,0,0,1,-3,2291,0,0,0,0,1,-3,1953,0,0,0,0,1,-1
6030   DATA  2201,0,0,1,0,1,2,1808,0,0,1,0,1,2,1849,0,0,1,0,0,-3
6040   DATA  1863,0,0,0,1,1,2,1829,0,0,0,1,1,2,1849,0,0,0,1,1,-3
6050   DATA  2070,1,0,0,0,1,-2,2174,1,0,0,0,1,-2,1553,1,0,0,0,0,2
6060   DATA  1760,1,0,1,0,1,-1,1656,1,0,1,0,0,1,1608,1,0,1,0,0,-2
6070   DATA  1766,1,0,0,1,1,3,1656,1,0,0,1,1,-1,2270,1,0,0,1,1,-1
6080   DATA  2070,0,1,0,0,1,-1,1697,0,1,0,0,1,2,1587,0,1,0,0,0,-1,1918,0,1,0,0,1,-1,1615,0,1,0,0,0,-1
6090   DATA  1725,0,1,1,0,1,1,1435,0,1,1,0,0,3
6100   DATA  1622,0,1,0,1,1,2,2270,0,1,0,1,1,-3,1849,0,1,0,1,1,2,1387,0,1,0,1,0,-3
6110   DATA  2132,1,1,0,0,1,3,1946,1,1,0,0,1,3
6120   DATA  1656,1,1,1,0,1,1,2270,1,1,1,0,1,3,1601,1,1,1,0,1,3
6130   DATA  1656,1,1,0,1,1,3,1898,1,1,0,1,1,3,1898,1,1,0,1,1,3
```

APPENDIX B

σ_f	X_1	X_2	X_3	X_4	X_5	X_6	X_7
2243	0	0	0	0	1.6	1	-3
2201	0	0	0	0	1.9	1	-3
2291	0	0	0	0	1.5	1	-3
1953	0	0	0	0	1.3	1	-1
2001	0	0	1	0	1.4	1	2
1808	0	0	1	0	2.2	1	2
1849	0	0	1	0	1.6	0	-3
1863	0	0	0	1	1.3	1	2
1829	0	0	0	1	1.7	1	2
1849	0	0	0	1	1.15	1	-3
2070	1	0	0	0	1.8	1	-2
2174	1	0	0	0	1.3	1	-2
1553	1	0	0	0	1.4	0	2
1760	1	0	1	0	1.4	1	-1
1656	1	0	1	0	0.95	0	1
1608	1	0	1	0	1.2	0	-2
1766	1	0	1	0	1.4	1	3
1656	1	0	0	1	1.35	1	-1
2270	1	0	0	1	1.84	1	-1
2070	0	1	0	0	1.1	1	-1
1697	0	1	0	0	1.15	1	2
1587	0	1	0	0	1.1	0	-1
1918	0	1	0	0	1.5	1	-1
1615	0	1	0	0	1.3	0	-1
1725	0	1	1	0	1.1	1	1
1435	0	1	1	0	0.7	0	3
1622	0	1	0	1	1.3	1	2
2270	0	1	0	1	1.88	1	-3
1849	0	1	0	1	1.72	1	2
1387	0	1	0	1	0.7	0	-3
2132	1	1	0	0	0.7	1	3
1946	1	1	0	0	1.2	1	3
1656	1	1	1	0	0.9	1	1
2270	1	1	1	0	1.3	1	3
1601	1	1	1	0	1.3	1	3
1387	1	1	1	0	0.7	0	2
1656	1	1	0	1	1.3	1	3
1898	1	1	0	1	1.3	1	3
1898	1	1	0	1	0.8	1	3

Determinant = 4.27393E+08

Beta term	Coefficient	90% Confidence Interval	95% Confidence Interval
0	1446.916		
1	54.56793	+/- 109.119	+/- 131.2581
2	-8.578278	+/- 122.1319	+/- 146.9112
3	-145	+/- 130.2102	+/- 156.6286
4	154.2864	+/- 120.954	+/- 145.4944
5	154.2864	+/- 181.4904	+/- 218.313
6	347.2718	+/- 137.1757	+/- 165.0073
7	-31.4109	+/- 27.20401	+/- 32.72343

Error Variance = 31914.84 with 31 D.F.
Error Standard Deviation = 178.6473
R - Squared = 0.6085253
Correlation Coefficient = 0.7800803

Y (Stress to failure-MPa)	Y - predicted (Stress to failure-MPa)	Difference	% Difference
2243	2135.578	107.4216	4.789195
2201	2181.864	19.13574	0.8694112
2291	2120.15	170.8501	7.457446
1953	2026.271	-73.27063	-3.751696
2001	1841.666	159.3342	7.96273
1808	1965.095	-157.095	-8.688881
1849	1682.806	166.1943	8.988337
1863	1786.738	76.26196	4.093503
1829	1848.453	-19.45264	-1.063567
1849	1921.15	-72.14966	-3.902091
2070	2189.493	-119.4927	-5.772593
2174	2112.35	61.65039	2.835805
1553	1654.463	-101.4629	-6.533348
1760	1990.766	-230.7662	-13.11172
1656	1511.044	144.9561	8.753384
1608	1644.148	-36.14819	-2.248022
1766	1825.224	-59.22364	-3.353547
1656	1943.553	-287.5531	-17.36432
2270	2019.154	250.8466	11.05051
2070	1986.835	83.16492	4.017629
1697	1900.017	-203.0169	-11.96328
1587	1639.563	-52.56336	-3.312121
1918	2048.55	-130.5498	-6.806559
1615	1670.421	-55.42066	-3.43162
1725	1818.312	-93.31238	-5.409414
1435	1346.304	88.6958	6.180892
1622	1778.16	-156.1599	-9.627615
2270	2025.201	244.7996	10.76412
1849	1842.96	6.039795	0.326652
1387	1495.871	-108.8706	-7.849359
2132	1853.645	278.355	13.05605
1946	1930.788	15.21191	0.7817017
1656	1842.023	-186.231	-11.23328
2270	1840.716	429.2842	18.9112
1601	1840.716	-239.7158	-14.97288
1387	1432.383	-45.38306	-3.27203
1656	1801.217	-145.2168	-8.76913
1898	1801.217	96.78321	5.099221
1898	1724.074	173.9263	9.16366

TECHNICAL REPORT INTERNAL DISTRIBUTION LIST

	NO. OF COPIES
CHIEF, DEVELOPMENT ENGINEERING DIVISION	
ATTN: AMSTA-AR-CCB-DA	1
-DB	1
-DC	1
-DD	1
-DE	1
CHIEF, ENGINEERING DIVISION	
ATTN: AMSTA-AR-CCB-E	1
-EA	1
-EB	1
-EC	1
CHIEF, TECHNOLOGY DIVISION	
ATTN: AMSTA-AR-CCB-T	2
-TA	1
-TB	1
-TC	1
TECHNICAL LIBRARY	
ATTN: AMSTA-AR-CCB-O	5
TECHNICAL PUBLICATIONS & EDITING SECTION	
ATTN: AMSTA-AR-CCB-O	3
OPERATIONS DIRECTORATE	
ATTN: SIOWV-ODP-P	1
DIRECTOR, PROCUREMENT & CONTRACTING DIRECTORATE	
ATTN: SIOWV-PP	1
DIRECTOR, PRODUCT ASSURANCE & TEST DIRECTORATE	
ATTN: SIOWV-QA	1

NOTE: PLEASE NOTIFY DIRECTOR, BENÉT LABORATORIES, ATTN: AMSTA-AR-CCB-O OF ADDRESS CHANGES.

TECHNICAL REPORT EXTERNAL DISTRIBUTION LIST

	NO. OF COPIES
ASST SEC OF THE ARMY RESEARCH AND DEVELOPMENT ATTN: DEPT FOR SCI AND TECH THE PENTAGON WASHINGTON, D.C. 20310-0103	1
DEFENSE TECHNICAL INFO CENTER ATTN: DTIC-OCP (ACQUISITIONS) 8725 JOHN J. KINGMAN ROAD STE 0944 FT. BELVOIR, VA 22060-6218	2
COMMANDER U.S. ARMY ARDEC ATTN: AMSTA-AR-AEE, BLDG. 3022	1
AMSTA-AR-AES, BLDG. 321	1
AMSTA-AR-AET-O, BLDG. 183	1
AMSTA-AR-FSA, BLDG. 354	1
AMSTA-AR-FSM-E	1
AMSTA-AR-FSS-D, BLDG. 94	1
AMSTA-AR-IMC, BLDG. 59 PICATINNY ARSENAL, NJ 07806-5000	2
DIRECTOR U.S. ARMY RESEARCH LABORATORY ATTN: AMSRL-DD-T, BLDG. 305 ABERDEEN PROVING GROUND, MD 21005-5066	1
DIRECTOR U.S. ARMY RESEARCH LABORATORY ATTN: AMSRL-WT-PD (DR. B. BURNS) ABERDEEN PROVING GROUND, MD 21005-5066	1
DIRECTOR U.S. MATERIEL SYSTEMS ANALYSIS ACTV ATTN: AMXSY-MP ABERDEEN PROVING GROUND, MD 21005-5071	1
COMMANDER ROCK ISLAND ARSENAL ATTN: SMCRI-SEM ROCK ISLAND, IL 61299-5001	1
MIAC/CINDAS PURDUE UNIVERSITY 2595 YEAGER ROAD WEST LAFAYETTE, IN 47906-1398	1
COMMANDER U.S. ARMY TANK-AUTMV R&D COMMAND ATTN: AMSTA-DDL (TECH LIBRARY) WARREN, MI 48397-5000	1
COMMANDER U.S. MILITARY ACADEMY ATTN: DEPARTMENT OF MECHANICS WEST POINT, NY 10966-1792	1
U.S. ARMY MISSILE COMMAND REDSTONE SCIENTIFIC INFO CENTER ATTN: AMSMI-RD-CS-R/DOCUMENTS BLDG. 4484 REDSTONE ARSENAL, AL 35898-5241	2
COMMANDER U.S. ARMY FOREIGN SCI & TECH CENTER ATTN: DRXST-SD 220 7TH STREET, N.E. CHARLOTTESVILLE, VA 22901	1
COMMANDER U.S. ARMY LABCOM, ISA ATTN: SLCIS-IM-TL 2800 POWER MILL ROAD ADELPHI, MD 20783-1145	1

NOTE: PLEASE NOTIFY COMMANDER, ARMAMENT RESEARCH, DEVELOPMENT, AND ENGINEERING CENTER, BENÉT LABORATORIES, CCAC, U.S. ARMY TANK-AUTOMOTIVE AND ARMAMENTS COMMAND, AMSTA-AR-CCB-O, WATERVLIET, NY 12189-4050 OF ADDRESS CHANGES.

TECHNICAL REPORT EXTERNAL DISTRIBUTION LIST (CONT'D)

	NO. OF COPIES
COMMANDER U.S. ARMY RESEARCH OFFICE ATTN: CHIEF, IPO P.O. BOX 12211 RESEARCH TRIANGLE PARK, NC 27709-2211	1
DIRECTOR U.S. NAVAL RESEARCH LABORATORY ATTN: MATERIALS SCI & TECH DIV WASHINGTON, D.C. 20375	1
WRIGHT LABORATORY ARMAMENT DIRECTORATE ATTN: WL/MNM EGLIN AFB, FL 32542-6810	1
WRIGHT LABORATORY ARMAMENT DIRECTORATE ATTN: WL/MNMF EGLIN AFB, FL 32542-6810	1

NOTE: PLEASE NOTIFY COMMANDER, ARMAMENT RESEARCH, DEVELOPMENT, AND ENGINEERING CENTER, BENÉT LABORATORIES, CCAC, U.S. ARMY TANK-AUTOMOTIVE AND ARMAMENTS COMMAND, AMSTA-AR-CCB-O, WATERVLIET, NY 12189-4050 OF ADDRESS CHANGES.